7-2013

Development of a physiologic ex vivo vessel perfusion system.

Mitchell J. Buller
University of Louisville

DEVELOPMENT OF A PHYSIOLOGIC *EX VIVO* VESSEL PERFUSION SYSTEM

By

Mitchell J. Buller, B.S.
University of Louisville, 2012

A Thesis
Submitted to the Faculty of the
Speed School of Engineering of the University of Louisville
as Partial Fulfillment of the Requirements
For the Professional Degree of

MASTER OF ENGINEERING

Department of Bioengineering
University of Louisville
Louisville, Kentucky

July 12, 2013

AN EX VIVO PERFUSION SYSTEM FOR BOVINE CAROTID ARTERIES

By

Mitchell J. Buller, B.S.
University of Louisville, 2012

A Thesis Approved on

_____
(DATE)

By the following Thesis Committee

_____
Steven C. Koenig, PhD, Thesis Director

_____
Guruprasad A. Giridharan, PhD – Thesis Advisor

_____
Stuart J. Williams, PhD – Thesis Advisor

_____
Mark S. Slaughter, MD – Thesis Advisor

_____
Kevin G. Soucy, PhD – Thesis Advisor

DEDICATION

This thesis is dedicated to my parents,

Mr. James M. Buller

and

Mrs. Ann C. Buller

ACKNOWLEDGMENTS

ABSTRACT

Introduction: Over time, continuous flow ventricular assist devices (VADs) have become the primary form of implanted mechanical circulatory support (MCS) due to their smaller size, higher energy efficiency, longer durability, and fewer LVAD-related complications when compared to pulsatile flow VADs. However, continuous and pulsatile flows may elicit different cellular and tissue response, particularly in the arterial vasculature, which could have a profound impact on the future operation of MCS devices. Therefore, a unique ex vivo perfusion system integrated with a mock adult circulatory system was design to study the impact of VAD-generated flow patterns on vascular function.

Methods: The benefits of a mock circulatory loop and an ex vivo perfusion system were combined by designing and integrating a vessel perfusion chamber to an adult-sized mock circulatory loop as a parallel flow branch distal to VAD outflow. Testing was conducted using a mock over several physiologic conditions (normal, heart failure, and hypertension) and at various levels of VAD flow. The system was integrated into an incubator to allow for control of pH and temperature in future studies and fitted with a vessel for feasibility testing. Data was collected using a custom Labview program and analyzed using the HEART program, an automated beat-to-beat cardiovascular analysis program based in Matlab.

Results: The chamber was successfully fabricated and installed in the mock circulatory system, allowing for perfusion and longitudinal stretching of bovine carotid arteries. The waveforms and values for pressures and flows created in the mock loop were similar to physiologic values under each tested condition. Under normal hemodynamic conditions (CO = 4.5 L/min, MAP = 91 mmHg) perfusion chamber flow was 0.51 L/min, while under HF conditions (CO = 3.3 L/min, MAP = 81 mmHg) it was reduced to 0.18 L/min, which are representative of in vivo carotid artery hemodynamics. Due to physiologic preloads and afterloads, VAD performance was as would be expected in clinical application. The system was found to be sufficient for future testing with bovine carotid arteries and extended perfusion times (>24 hours).

Conclusions: This study resulted in an ex vivo vessel perfusion system that can successfully expose bovine carotid arteries to physiologic and VAD-specific hemodynamic waveforms. The ability to combine the mock ventricle with clinically implanted VADs makes this system both unique and clinically relevant for studying the effects of continuous versus pulsatile flow on the peripheral vasculature.

TABLE OF CONTENTS

LIST OF TABLES

LIST OF FIGURES

CHAPTER I – INTRODUCTION

A. <u>Heart Failure</u>

An estimated 5.1 million Americans over the age of 20 are currently living with heart failure[6], while over 200,000 of that population have refractory end-stage heart failure with a mortality rate of 70% - 90%[7]. That number is expected to increase by 25% by the year 2030. Cardiovascular disease is also costly, as it is projected to incur $358 billion in medical expenses in 2015, with that number climbing to $818.1 billion by 2030. Congestive heart failure (CHF) alone accounts for $32.4 billion and $77.7 billion of those figures, respectively, or approximately 9% of the total cost. These numbers indicate that CHF is a disease that warrants continued research and attention.

CHF occurs when blood backs up in other areas of the body due to ineffective pumping of the heart[8]. This ineffectiveness can result from systolic failure, when the heart is too weak to eject a sufficient volume of blood, or diastolic failure, when the cardiac muscle becomes stiff and does not fill with blood easily. Typically, CHF results from a combination of these deficiencies and thus prohibits the heart from delivering sufficient amounts of oxygen-rich blood to the body due to decreased pressures and compliances throughout the cardiovascular system.

As CHF progresses, the body initiates a multitude of compensatory mechanisms in varying degrees. The Frank-Starling mechanism allows the heart to change its

force of contraction and therefore stroke volume in response to venous return[9].

In CHF, this mechanism can have potentially adverse effects, leading to

ventricular dilation and increased heartrate. Several neurohumoral responses

are also initiated, such as the activation of the sympathetic nerves, the renin-

angiotensin system of the kidneys, and increased release of antidiuretic hormone

and atrial natriuretic peptide. These mechanisms result in increased fluid

retention and edema, leading to arterial vasoconstriction, venous constriction,

and increased blood pressure.

B. Treatment Options

The most effective long-term remedy for CHF is a heart transplant.

Unfortunately, less than 2,400 such procedures are performed in the United

States each year due to a widespread shortage of available donor organs

(**Figure 1**). The number of annual heart transplants has been consistent for

over 20 years, even in spite of the increasing HF diagnoses. For the remaining

end-stage HF patients who are unable to receive a transplant due to lack of

donor organs, age, or other comorbidities, additional treatment methods must be

utilized.
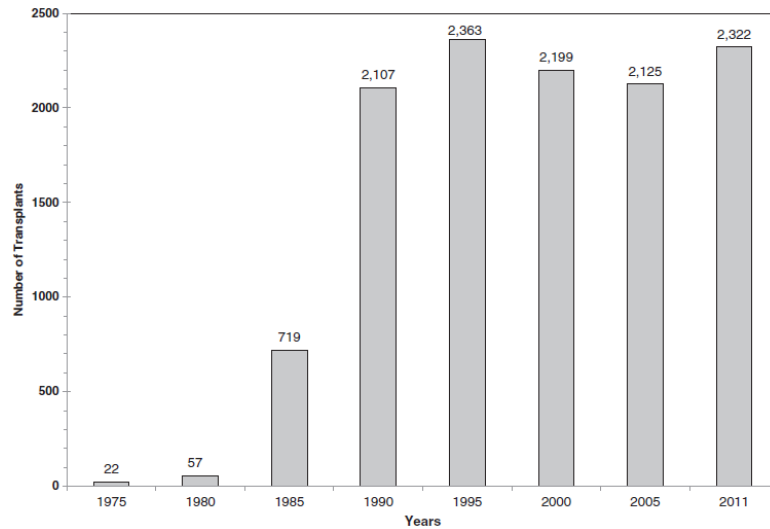
Figure 1. Trends in heart transplantations in the U.S.[6]

For patients suffering from New York Heart Association (NYHA) Class I and Class II heart failure, proper medical management is the first step in effectively managing its symptoms. Two common classes of medications prescribed in the treatment of heart failure are inotropes and beta-blockers. Inotropes are used to alter the force of cardiac muscle contraction by either weakening the contractions (negative inotropes) or strengthening them (positive inotropes)[10]. Examples include epinephrine, norepinephrine, and dobutamine. Beta-blockers reduce the workload on the heart and dilate your blood vessels, causing your heart to beat slower and with less force[1]. These medications are often best used in combination and supplemented with diuretics and ACE inhibitors.

When patients enter the NYHA Class III and IV stages of heart failure and proper medical management is not enough to combat their severe limitations in activity, mechanical circulatory support (MCS) must be considered. The original form of MCS was the cardiopulmonary bypass (CPB) machine, in which a series of

external roller pumps takes over the heart's blood-pumping function while the blood is simultaneously oxygenated extracorporeally. Fully implantable devices known as ventricular assist devices (VADs) were later developed. VADs provided more prolonged periods of MCS outside of the hospital.

The first generation of VADs were introduced in the late 1970s and consisted of bulky, pneumatically driven pumps, such as the HeartMate XVE (Thoratec Corp., Pleasanton, CA) and the Novacor LVAD (Novacor Corp., Oakland, CA), that produced pulsatile flow (PF) patterns. Like most VADs, these pumps were designed to supplement the function of a single ventricle, typically the left. Despite the restrictive size and associated risks with early generation PF VADs, clinical management of HF with these devices was largely successful and established VADs as an effective option for late-stage HF patients.

This second generation of VADs, led by the HeartMate II (Thoratec Corp., Pleasanton, CA) and the HVAD (HeartWare, Inc., Framingham, MA), gained widespread clinical acceptance after the turn of the century due to their smaller pump size and driver size, increased reliability, and improved efficiency. Improvements on this technology have allowed for even smaller and less invasive devices to be developed. Still other devices in development include the third generation of VADs, such as the HeartMate III (Thoratec Corp., Pleasanton, CA), that are CF but have the capability to produce PF through various algorithms currently under development.

C. Effects of VADs

As previously mentioned, CF VADs have become the primary form of implanted MCS for several reasons. First, their smaller size allows them to be more easily implanted in the thoracic cavity. CF VADs have also demonstrated higher energy efficiency, longer durability, and fewer post-surgical LVAD-related complications when compared to their PF counterparts[11]. However, the effects of continuous versus pulsatile flow on the body continue to be studied and could have a profound impact on future MCS device technologies.

The effects of flow patterns can be seen on various levels of bodily organization, from the cellular level, to the vascular level, and finally to the level of organ systems and their interactions. On a cellular level, pulsatile flow has been shown to reduce endothelial damage compared to nonpulsatile flow[12] and possibly suppress the release of potentially harmful cyotkines[13, 14]. Increased pulse pressure from pulsatile flow in baroreceptor units has been shown to decrease systemic vascular resistance[15] and the frequency-dependent component of these baroreceptors can be altered during different hemodynamic conditions[16] Studies also show that the endothelial release of nitric oxide, a key cellular component in cardiovascular function, in the peripheral vasculature is enhanced by pulsatile flow[17].

On a vascular level, the effects of critical shear stresses can be seen through the activation and manipulation of several different biological mechanisms within the

vasculature, which are induced by two types of mechanical stretch in the vessels[18, 19].   These changes can have long term effects on endothelial-mediated vascular adaptive mechanisms[20]. Moreover, nonpulsatile flow in a total artificial heart experiment has been shown to cause narrowing and rarefaction in the microcirculatory network, causing dystrophy in samples from the lungs, liver, and kidneys[21].

Those microcirculatory effects can lead to changes in end-organ behavior stemming from the varying flow patterns. In the kidneys, short-term results seem to favor the use of pulsatile flow[22], while long-term continuous flow obtains better renal perfusion than short-term usage and is not technically inferior to pulsatile flow [23]. Studies conducted on the liver show that pulsatile flow sustains total hepatic blood flow more effectively than continuous flow, due to the specific preservation of hepatic arterial and portal venous blood flow (attributed to prevention of hepatic arterial vasoconstriction)[24]. Similar impact was reported in the neurological system, in that lower vascular resistance and higher flow rates were associated with pulsatile versus nonpulsatile flow[23, 25]. Studies conducted on the gastrointestinal (GI) system are concerning, where data has shown that continuous flow is significantly more likely to cause GI bleeding than pulsatile flow, with a near ten-fold incidence difference in some cases[26].

Among many others, these findings have driven a growing movement by researchers to determine whether pulsatility is truly needed in the human cardiovascular system and, if so, to what degree it is needed. While studies are

being conducted to investigate the need for this pulsatility[27], the VAD industry

and engineers are preemptively developing PF algorithms for current and next-

generation CF VADs[28]. In order to test the biologic responses to these highly-

specialized VAD flow patterns with adequate scientific rigor and accuracy,

specialized flow simulation systems must be developed.

D. Mock Circulatory Loops

A common method of mimicking *in vivo* flow conditions for the study of various

flow patterns and/or MCS devices is the mock circulatory loop. These loops

begin with a source of flow, typically a mock ventricle driven pneumatically or

with a piston[29]. Compliance chambers for arterial and/or venous compliance

adjustment are typically used[30], along with some sort of adjustable resistance to

account for systemic and pulmonary vascular resistance[31]. Connections are made

via polypropylene or other plastic tubing. While the components seem basic,

mock circulatory loops can be modified via any number of components or

configurations to study many different circulatory scenarios.

Many mock loop systems are created in order to be able to adapt to test the

various types of MCS devices[32-37]. Other systems are more complex and

specified, such as those used to study a pediatric circulation[38, 39] or the

associated Norwood procedure[40] and Fontan circulation[41]. Still others are used

to develop and verify the aforementioned pulsatile flow patterns produced by

continuous flow VADs[42-44].

This diversity and adjustability is one of the main advantages of mock circulatory systems. Not only can these systems be set up to mimic various types of circulation, but the compliance, resistance, preload, afterload, and other included parameters can be adjusted to create a multitude of different cardiovascular conditions, such as hypertension or heart failure. Devices ranging from VADs[33], to TAHs[43], to IABPs[36] can be included, as well as other prostheses[37]. Fluids of varying viscosities, such as water, glycerol, or blood can be utilized to achieve desired viscosities. Mock circulatory loops enable the user to instantaneously change hemodynamic conditions and spare the lives of animals that would typically be experimented on, while also being more cost efficient and reproducible than said animal experiments.

The biggest disadvantage of these systems is that they are only models, and assumptions must inherently be made and accounted for. However, systems with increased complexity are able to account for more variables and therefore can provide highly accurate models of natural hemodynamic conditions.

One such system is the standard mock loop setup used by investigators at the Cardiovascular Innovation Institute (CII). The standard setup consists of a silicone left ventricle pneumatically driven by an external driver, aorta, arterial resistance and compliance, and venous reservoir. These elements are connected using plastic tubing connectors and flexible ¾" silicone tubing. Ventricular pressure, heart rate, resistances, and compliances can be adjusted to reproduce hemodynamic pressure and flow waveforms of the physiology of an adult human

in several distinct conditions: normal, heart failure, and hypertension. Aortic and

LVAD flows are measured using in-line and clamp Transonic Flow Probes

(Transonic Systems, Ithica, NY), respectively. Aortic and left ventricular

pressures are measured using single-tipped Millar pressure catheters (Millar

Instruments, TX). One of two pneumatic ventricle drivers can be used (LB

Engineering, Germany; Thoratec Corp., Pleasanton, CA). These drivers enable

the modification and adjustment of key parameters such as ventricle systolic and

diastolic time periods and pressure, vacuum, and motor percentages.

E. *Ex vivo* Perfusion Systems

Ex vivo perfusion systems are another tool with a multitude of uses. As the name

implies, these systems involve the perfusion of blood or another nutrient-rich

substance throughout a group of cells, tissue, or an organ in an environment

outside the body. These systems come in a wide range of sizes, from smaller

systems for the perfusion of cell cultures to large configurations for the perfusion

of entire organs.

Two transplanted organs that are often perfused are the lungs and kidneys.

Lungs can be perfused for 4-6 hours prior to transplant[45], often

normothermically[46, 47] and in combination with static cold preservation to remedy

the effects of warm ischemia[48]. This *ex vivo* lung perfusion has proven to be an

effective way to help separate 'good' lungs from a previously rejected pool to

assist with the shortage of donor lungs[49]. Specific interest lies in the area of

9

donation after circulatory death[46, 50]. In terms of kidneys, simple systems of normothermic perfusion immediately prior to transplant have been effective after prolonged periods of static cold storage[51]. Because of this success, perfusion of kidneys with various substances has been studied[52, 53]. Other *ex vivo* perfusion systems have involved liver REFs, cirrhotic tissue REF, mouse placentas REF, and even bone REF, among others[54-61].

It is not surprising that *ex vivo* perfusion systems for cardiovascular tissues are extensively used in scientific research. Specifically, researchers have developed various systems for the perfusion of hearts. As with other organs, the primary focus is preparing hearts for transplant[62, 63]. Some systems have utilized animal hearts in order to develop tools to assess the viability of hearts for transplant[64-67]. While different parameters for evaluating the potential hearts are being determined[68, 69], the effects of various parameters on the peripheral vasculature are also being examined.

Like all *ex vivo* perfusion systems, these vascular perfusion systems can also vary widely in size, beginning with smaller microfluidic systems used for the perfusion of vascular endothelial cell cultures. These types of systems are useful for identifying the effects of pulse waves on a cellular level and use similar components to mock circulatory loops, such as pulsatile blood pumps and flow meters[70]. Unfortunately, these systems can typically only study a specific cell type, as opposed to the effects of flow on an entire vessel or organ.

More advanced systems attempt to mimic vessels by culturing vascular cells in flexible rubber tubing[71, 72]. These systems are able to moderate shear stress levels[72] and even mimic disease states[71], but are unable to generate physiologic waveforms or waveforms associated with pathologic conditions. Additional systems are also able to produce pulsatile flow patterns, but only incorporate static cell cultures and have issues with retrograde flow and shear stress and strain measurements[73, 74].

Similar to static culture protocol, *ex vivo* perfusion of blood vessels requires them to be cultured at physiologic temperature and pH, and with appropriate culture medium with antibiotic and antifungal agents, with the added parameter of being exposed to various flow patterns. Systems are typically driven via peristaltic pumps[75-78] in order to mimic various pulsatile flow waveforms. They typically utilize precise pressure, flow, and gas exchange control to measure a variety of endpoints, such as fluid mechanical forces[75, 76] and biological marker expression[78-82]. Some even have unique abilities like the capacity for longitudinal stretch[77, 79] or the measurement of vessel diameter[80, 83]. Like mock circulatory loops, these systems are highly adaptable and can be modified to support a variety of research needs.

F. Purpose of the Research

Although the effects of mechanical stimulation to the vasculature have been extensively studied, the response to CF VAD-generated continuous flow and

pulsatile flow profiles has not been examined. This project combines the advantages of a mock circulatory loop with those of an *ex vivo* perfusion by attaching a vessel within the mock loop and exposing it to those unique flow profiles. By mimicking the complexity of the physiologic *in vivo* environment by using the combination of a pneumatic ventricle and VAD in series, this system is capable of providing valuable information on the effects of continuous and pulsatile flow on the peripheral vasculature.

The *ex vivo* perfusion system in this project will be able to accept a bovine carotid artery in order to accurately mimic *in vivo* conditions. The chamber will be able to be integrated into a mock adult circulatory flow loop, and the system will include design features for temperature control, pH regulation, media exchange, and sterilization.

The research performed in this thesis project accomplishes several aims. An *ex vivo* perfusion chamber is designed and integrated into the mock loop to prove feasibility of the system. Physiologic, pathologic, and mechanically-altered hemodynamics are created. Finally, the mock circulation system is reduced and re-designed for tissue culture considerations. In addition, improvements to the perfusion chamber are presented, which are ready for fabrication and implementation with future studies.

The vessel chamber for the artery is watertight, with cannulas at each end to attach the vessel and three ports for fluid exchange, ventilation, and proper gas

exchange. The system is adjustable in length to allow for proper vessel stretching and is completely sterilizable.

Once the chamber was completed, the mock circulatory loop was modified for integration of the perfusion system in order to demonstrate that physiologic flows and pressures can be achieved. First, the chamber was integrated with only the mock ventricle to demonstrate normal physiologic pressures and flows. The CF VAD (HVAD, HeartWare Corp., Framingham, MA) was then added to demonstrate typical flows of the VAD in conjunction with the native ventricle. Finally, the pulsatile flow algorithm was implemented and data was collected. The mock loop system was then transferred to an incubator to achieve physiologic temperature and pH, as described in the following section.

CHAPTER II – MATERIALS AND METHODS

A. *Ex vivo* Vessel Perfusion Chamber

The *ex vivo* vessel perfusion chamber was created using a 100 mL syringe of

inner diameter 1.4 inches. The tip was first cut off to create a hollow tube of

length 4.8 inches. Three holes were drilled in the side of the tube: two to allow

for fluid recirculation and one to vent. Luer lock ports were then fixed in each

hole and capped. The handles of two syringe plungers were then removed so

that only the rubber end was intact. A hole was drilled in each plunger to allow

for the insertion of a ¼" to 3/16" plastic tubing connector. One end of each

connector was connected externally to ¼" silicone tubing, while the end on the

inside of the chamber was connected to the vessel. Because no actual vessels

were used in this study, a piece of 3/16" tubing was used to simulate the vessel

for the preliminary design. In hemodynamic verification studies, a section of

penrose drain was used, as it better mimicked the elasticity of a natural vessel.

The prototype can be seen in **Figure 2**.

Figure 2. Prototype of vessel perfusion chamber

B. Mock Circulatory Loop

For the purpose of this study, several modifications were made to the standard
mock circulatory system to allow for testing of the carotid artery. The *ex vivo*
vessel perfusion chamber with the mock carotid artery, as described in the next
section, was placed in a looped branch after the proximal compliance chamber.
While a connection of the branch between the arterial and venous sides was
considered, as this would be more physiologically accurate, the resulting system
would likely require an additional compliance chamber and fluid reservoir, adding
to the overall complexity of the system. A second compliance chamber was
added to represent the additional compliance of the carotid artery branch. The
remainder of the system remained physically unchanged. An additional clamp
Transonic Flow Probe (Transonic Systems, Ithica, NY) was placed just promixal
to the vessel chamber to measure carotid artery pressure and an additional

15

single-tipped Millar pressure catheter (Millar Instruments, TX) was placed just distal to the chamber to measure carotid artery flow. A block diagram of the system can be seen in **Figure 3**, as well as the complete setup in **Figure 4**.
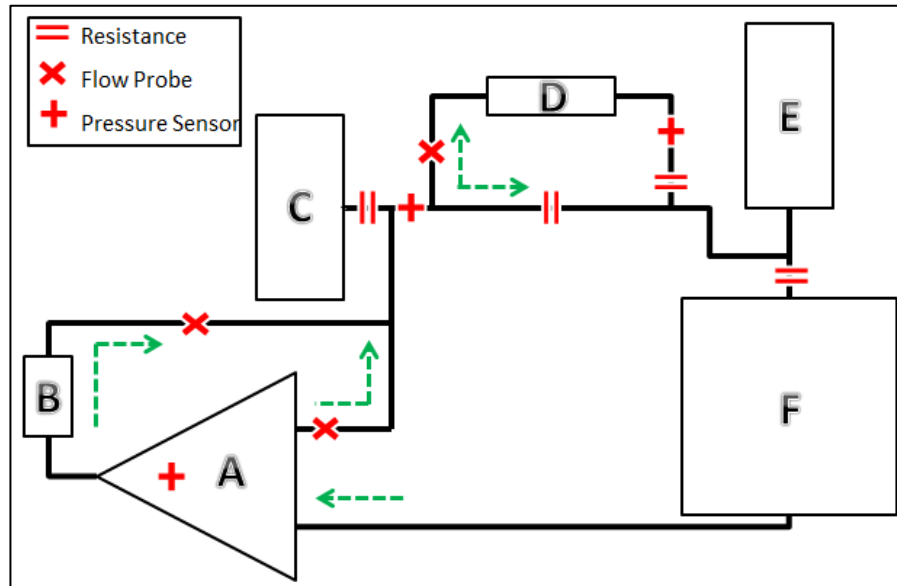
Figure 3. Block diagram of modified mock circulatory loop with components: A. pneumatic ventricle, B. VAD, C. proximal compliance, D. vessel chamber, E. distal compliance, and F. volume reservoir.
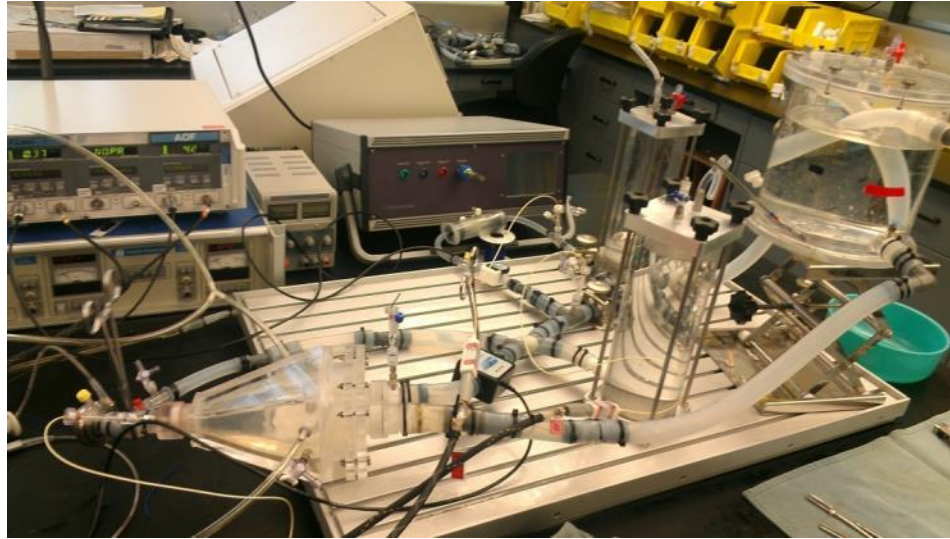
Figure 4. Complete setup of modified mock circulatory loop

One of the key advantages of this *ex vivo* arterial perfusion system is the ability to integrate various MCS devices into the circulation, including several types of LVADs and counter-pulsation devices. For the purposes of this study, the LVAD used was the centrifugal flow HVAD by HeartWare (Miami Lakes, FL). For the first portion of the experiment, the standard controller was used to provide continuous flow to the system.

However, the second portion of the experiment involved the use of a pulsatile flow algorithm for the pump. For this purpose, a controller was programmed by engineers at HeartWare under the direction of the investigators to enable LVAD pump speed modulation (**Figure 5**). The program enabled the user to alter the degree of pulsatility by changing three parameters: the change in RPM (amplitude), the time period, and the time interval between pulses. This

controller allowed for the creation of pulsatile waveforms from the continuous

flow HVAD to test the carotid artery under various flow conditions.

Figure 5. Screenshot of HVAD pulsatility controller

C. Incubator Integration

For additional testing, the mock circulatory system was integrated into the

incubator (Isotemp, Fischer Scientific) in order to prepare the system for testing

under physiologic pH and temperature with actual carotid arteries. The lack of

space in the interior made some slight modifications necessary, including the

shortening of tubing lengths and the fixation of the fluid reservoir at a fixed

height. A new fluid reservoir was also fabricated from a shallow plastic bin to

allow it to be placed on the top shelf of the incubator. The complete setup can

be seen in **Figure 6** and a full schematic is attached in **Appendix A**. Once

integrated, data sets were collected at the same physiologic conditions as the

initial testing to demonstrate similar performance of the system in its new

configuration.

Figure 6. Incubator testing setup

D. Testing

After the creation of the vessel chamber, testing was conducted using the

aforementioned mock circulatory system. First, data was collected under normal

physiologic conditions without the inclusion of the HVAD. This data was

collected at varying levels of pressure and flow in an attempt to match target values and waveforms (**Table 1**). The HVAD was then included and data sets were collected for heart failure and hypertension conditions at the following levels of VAD flow: no flow, low flow, medium flow, and high flow. Low flow was defined as 2000 rpm. High flow was defined as 3200 rpm according to the high rpm setting used clinically by physicians associated with the CII. Medium flow was then taken as the midway point between low and high flow, 2600 rpm. The heart failure condition was created by increasing the compliance to reduce pulse pressures and decreasing the drive pressure and increasing the preload to simulate a dilated left ventricle and increase left ventricular end-diastolic pressure. The hypertensive condition was created by increasing resistance and decreasing compliance to simulate stiffening of the arteries.

Table 1. Target blood pressures for hemodynamic states[1-5]. Values without literature references were extrapolated from known values in other conditions.

Hemodynamic Condition	AoP (mmHg)			CdAP (mmHg)			CdAF (L/min)	AoF (L/min)
	Systolic	Diastolic	Pulse	Systolic	Diastolic	Pulse		
Normal	120	76	44	100	65	35	0.24 - 0.66	4.70
Heart Failure	97	60	37	81	51	30	0.17 - 0.49	3.50
Hypertension	>140	> 90	50	> 117	> 77	40	0.15 - 0.42	3.00

In the second round of testing, after integration into the incubator, additional levels of flow were added. A 'full flow' VAD condition set at 3800 rpm was added in an attempt to significantly reduce any remaining pulse pressure and completely unload the ventricle. Prior to the administration of pulsatile flow

algorithms, a modified heart failure condition was created to match the exact parameters used in previous work[84]. Pulsatile flow algorithms at 2900 +/- 1100 rpm and 3200 +/- 800 rpm were then added. As detailed previously[85], the first condition allowed for the maximum rpm modulation, while the second condition provided full unloading of the ventricle. These two conditions were run both asynchronously at periods of 0.4, 0.5, 0.8, and 1.6 seconds and synchronously. In order for this to be accomplished, the cardiac cycle on the ventricle driver was set at 0.8 seconds and at 0.79 seconds on the VAD controller. This allowed the VAD to drift from phases of co-pulsation to counter-pulsation over a two minute data set. Co-pulsation occurs when the VAD produces flow at the same time the ventricle is contracting, whereas counter-pulsation occurs when the VAD produces flow when the ventricle is filling. The difference can be observed in the offset between the pulses of the aortic and left ventricular pressures. In co-pulsation, a zero degree offset exists between the pulses, whereas a 180 degree offset exists in counter-pulsation.

In the final round of testing, a bovine carotid artery (1/8" diameter) was incorporated into the system (**Figure 7**) in the vessel perfusion chamber to prove feasibility of the system. No vessel viability testing was conducted, but similar conditions as in the first two testing sets were replicated. Specifically, baseline normal and heart failure conditions were established, followed by several data sets of continuous and pulsatile VAD flow.
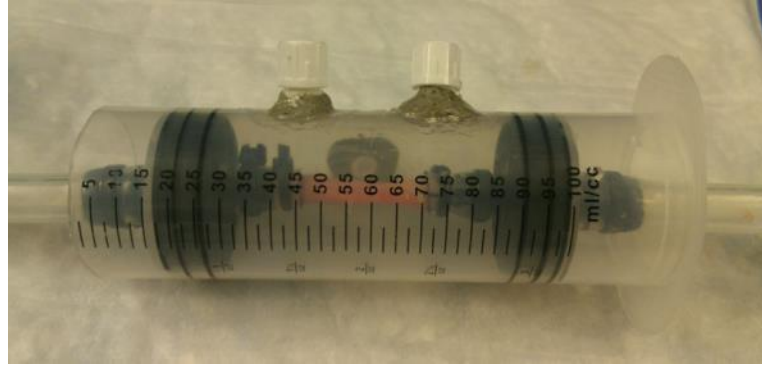
Figure 7. Bovine carotid artery integrated into vessel perfusion chamber

E. Data Collection and Analysis

Data was collected using a custom Labview program designed by investigators at the CII. This program allows for the display of up to 9 pressures and flows and the acquisition of data sets of any size. In this study, the parameters recorded were left ventricular pressure, aortic pressure, carotid artery pressure, aortic flow, VAD flow, and carotid artery flow. Data sets of 15 or 30 seconds in length were acquired during bench top testing and for the basic hemodynamic and CF VAD conditions in incubator testing. For the asynchronous pulsatile VAD flow modulation data sets, data sets ranging from 12 – 48 seconds were taken in order to record 15 'beats' of the VAD. For synchronous VAD data sets, data sets of two minutes were taken in order to record periods of both co-pulsation and counter-pulsation. Prior to the commencement of each data set, the circulatory loop was run for 20 – 30 seconds to achieve a steady state for each condition. The data was analyzed using the HEART program, an automated beat-to-beat cardiovascular analysis package using Matlab[86], along with additional custom

Matlab programs developed for the analysis of pulsatile VAD waveforms[85]. This

beat analysis allowed for the calibration of data channels, the calculation of

various peaks, averages, and pulses, and the creation of data plots. Four second

plots of pressure and flow waveforms were plotted to provide a snapshot of the

data sets.

CHAPTER III – RESULTS

A. <u>Bench Top Testing Results</u>

Initial testing of the *ex vivo* arterial perfusion system was successful in

replicating physiologic and pathologic (heart failure and hypertension) waveforms

for various pressures and flows. Target pressure and flow parameters are listed

in **Table 1**. Resistance, compliance, and ventricle driver settings were first

adjusted to create a baseline condition (no VAD) representing normal

cardiovascular parameters (**Figure 8**). It should be noted that large spikes in

pressure and flow will appear due to ringing of the mechanical aortic and mitral

valves. Baseline aortic flow (AoF) was kept at approximately 4.0 L/min to

represent a normal cardiac output. Normal average pressures of 95 mmHg for

AoP and 86 mmHg for CdAP were also obtained. The baseline condition was

followed by data sets of low, medium, and high VAD flow to verify proper

functionality of the VAD and perfusion system setup (**Appendix A**).
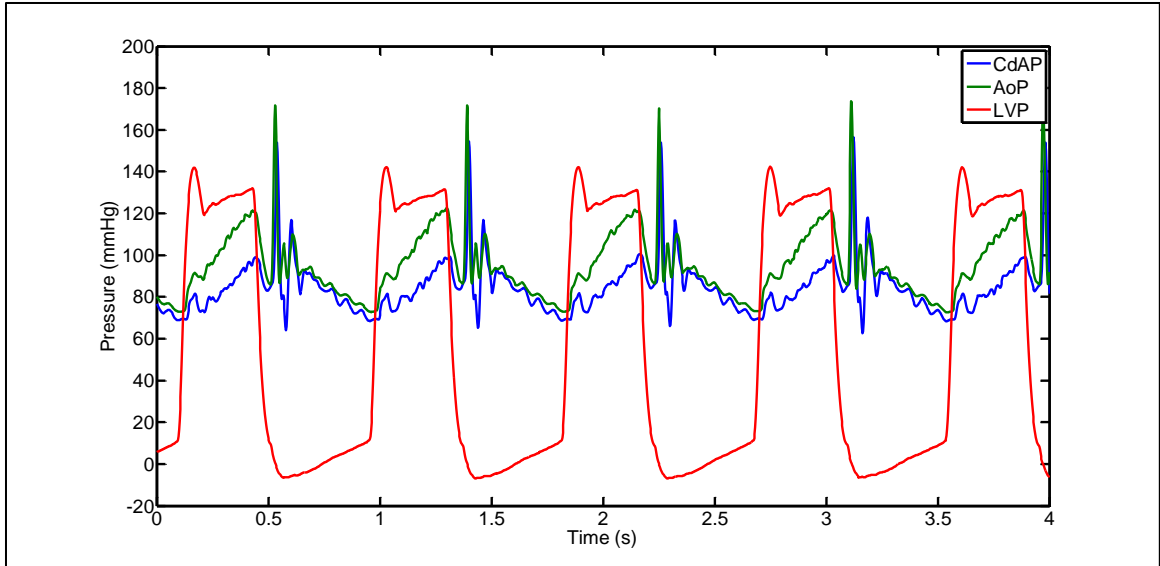
Figure 8. Baseline pressures

Next, a heart failure condition was created. At the onset of the heart failure condition, left ventricular end-diastolic pressure rose (**Figure 9**). This resulted in an overall decrease in pressures. Mean AoF decreased to 3.3 L/min, while mean CdAF decreased to 0.18 L/min.
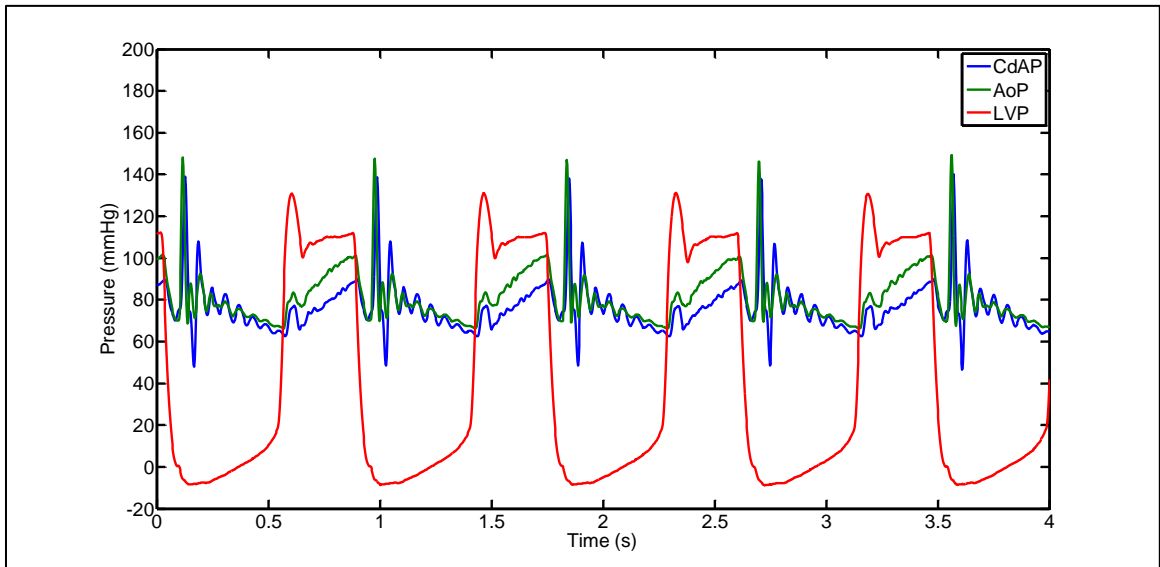
Figure 9. Pressures in heart failure condition

Similar to the hypertensive condition, pressures and flows increased with increasing VAD support until the ventricle became fully unloaded (**Figure 10**). However, AoF dropped below zero due to the elimination of flow through the aortic valve with increased ventricular unloading along with some slight retrograde flow due to the mock loop setup (**Figure 11**).
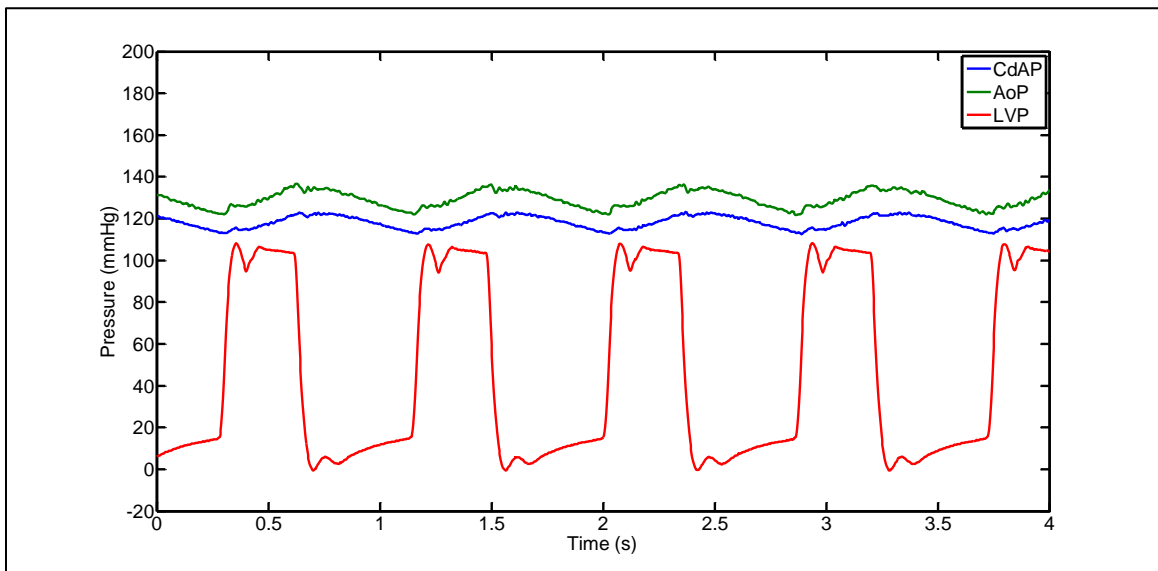
Figure 10. Pressures in heart failure condition with high VAD flow
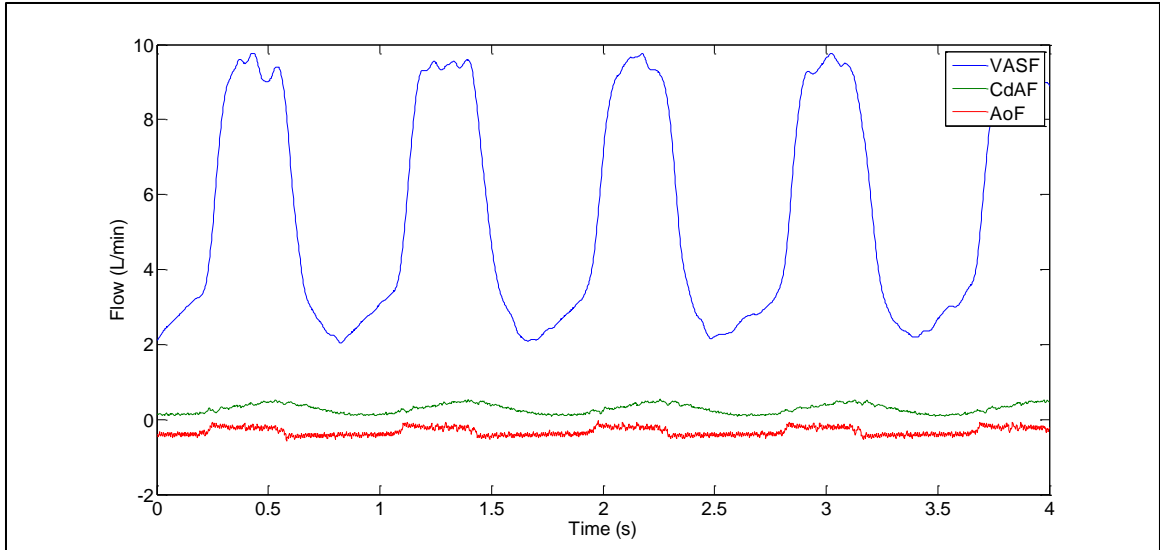
Figure 11. Flows in heart failure condition with high VAD flow

After an additional baseline condition was created to restore normal function, a hypertensive condition was created (**Figure 12**). This resulted in higher pressures, including higher pulse pressures for the aorta and carotid artery, caused *in vivo* by the stiffening of the vascular walls. Due to the increased resistance, mean AoF was decreased to approximately 3 L/min and mean CdAF to 0.12 L/min, values that were slightly below literature references (**Table 2**).
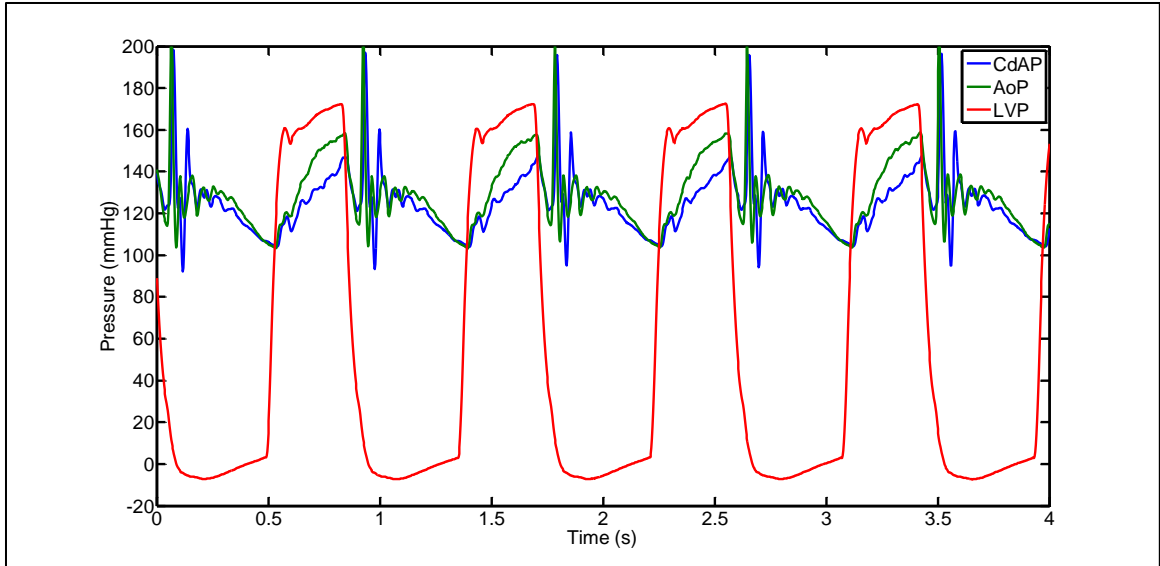
Figure 12. Pressures in hypertensive condition

Again, data sets of low, medium, and high VAD flow were taken to simulate VAD function in a hypertensive condition. Pressures increased, likely due to the increased flow through the vessels (**Figure 13**), as the major hemodynamic effect of VAD support is increased pressure and flow[87]. Mean AoF decreased with increasing VADF as more of the flow bypassed the aortic valve and went through the VAD and the ventricle became increasingly unloaded (**Figure 14**).

28
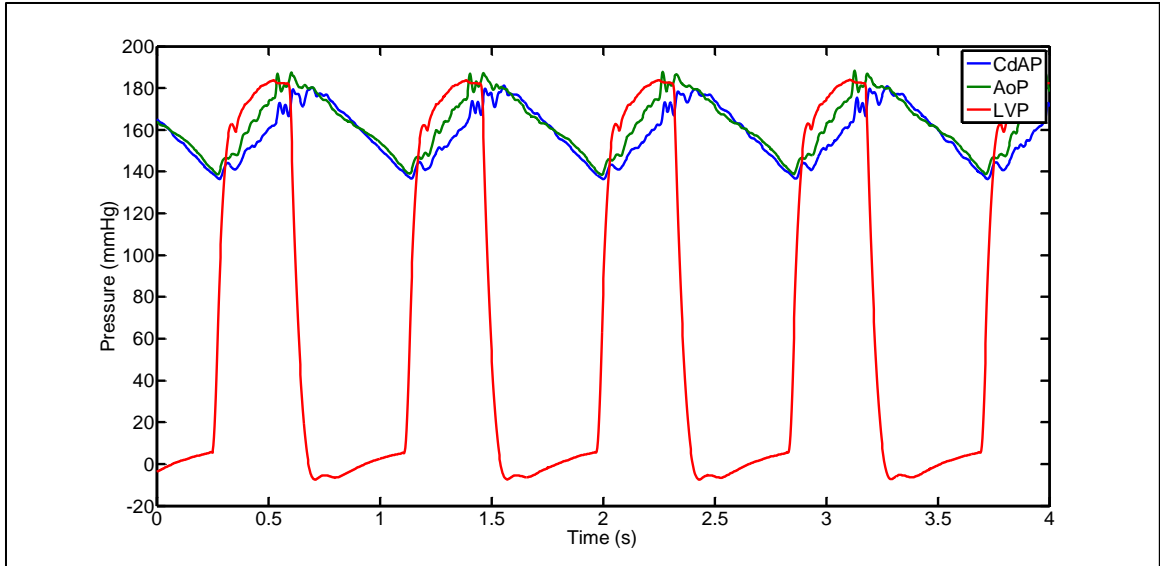
Figure 13. Pressures for hypertensive condition with high VAD flow
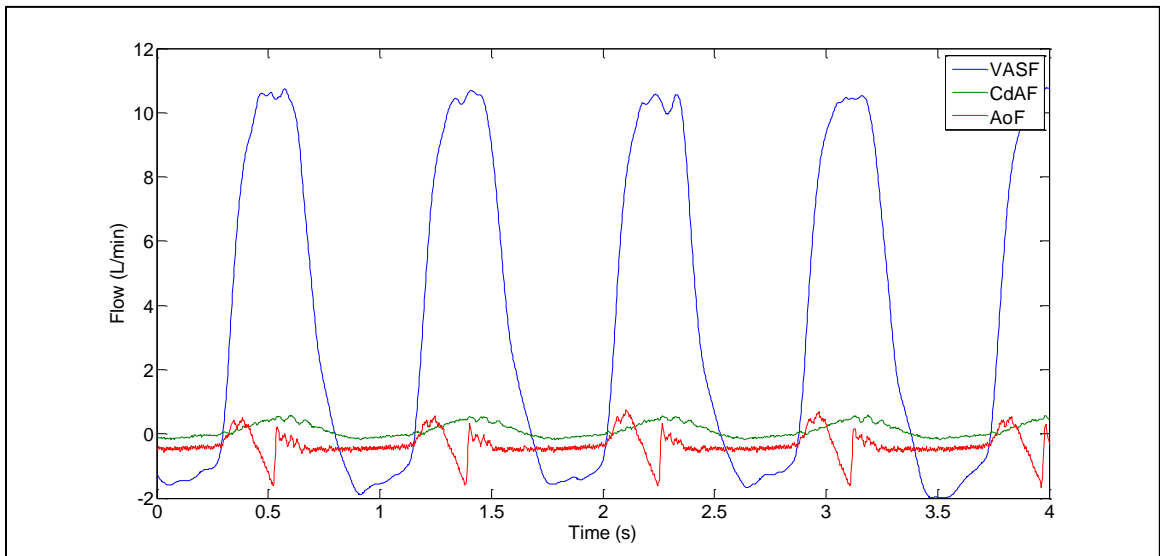
Figure 14. Flows for hypertensive condition with high VAD flow

In terms of the behavior of the carotid artery branch, the perfusion system was able to attain pressure and flow values near the target values. While the values for the maximum and average carotid flows and pressures were able to be

29

obtained (**Table 2**), waveform morphology for the CdAF differed slightly from

published figures[4, 88, 89].

Table 2. Carotid artery pressures and flows in bench top testing versus target

values. Values were obtained from figures due to influence of valve ringing in

data analysis. Bolded values fall within 10% sensor error range of target values.

Hemodynamic Condition	Target Values				Obtained Values			
	CdAP (mmHg)			CdAF (L/min)	CdAP (mmHg)			CdAF (L/min)
	Systolic	Diastolic	Pulse		Systolic	Diastolic	Pulse	
Normal	100	65	35	0.24 - 0.66	**98**	**69**	29	0.20
Heart Failure	81	51	30	0.17 - 0.49	**85**	59	26	**0.18**
Hypertension	> 117	> 77	40	0.15 - 0.42	**140**	**100**	**40**	0.12

B. Incubator Testing Results

Once the *ex vivo* arterial perfusion system was transferred from the bench top to

the incubator, the first goal of testing was to reestablish proper pressure and

flow waveforms for baseline, heart failure, and hypertensive hemodynamic

conditions (**Figures 15-17**).
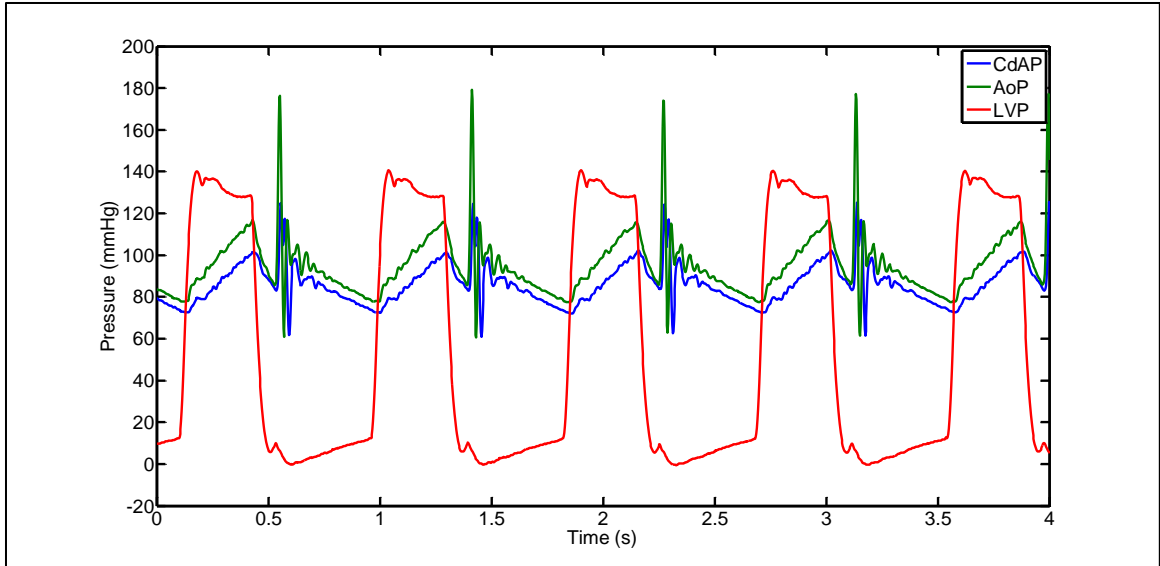
Figure 15. Pressures in baseline condition
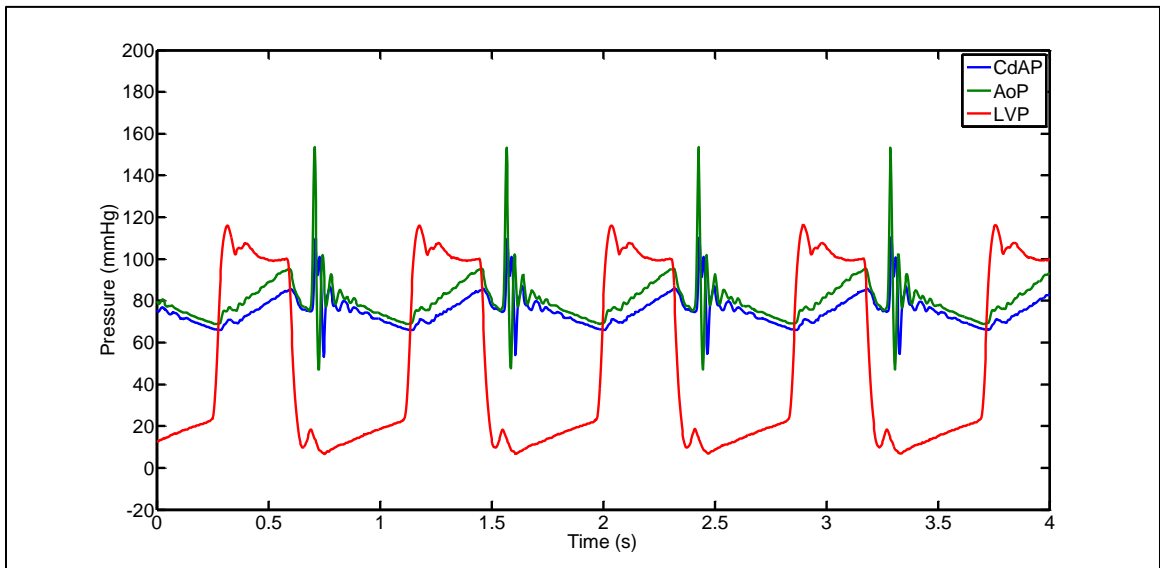
Figure 16. Pressures in heart failure condition

31
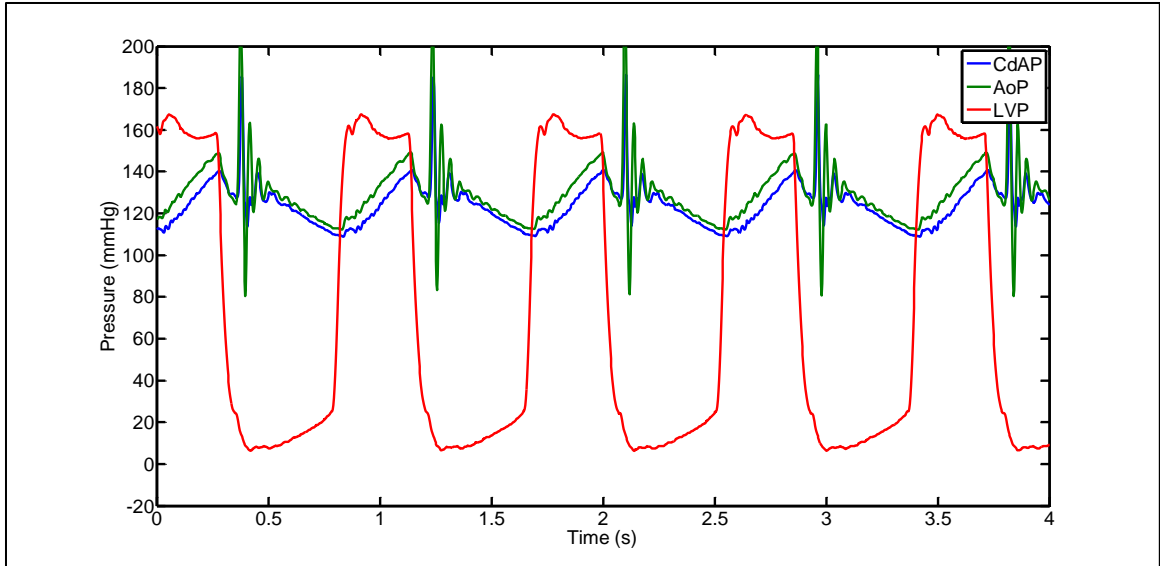
Figure 17. Pressures in hyptertensive condition

After each of these basic conditions were established, four levels of VAD support were tested under each condition. The three levels used in the initial testing were replicated along with the addition of the aforementioned 'full VAD' condition, in which the VAD was set to 3800 rpm in order to fully unload the ventricle and reduce or eliminate any pulse pressures. As expected and observed in the initial testing, the pulse pressures were reduced as the level of CF VAD support increased to full ventricular unloading (**Figure 18**). However, they still remained slightly higher than the pulse pressures that have been observed in clinical VAD patients, which can drop as low as 3 – 5 mmHg, although pulse pressures are often kept between 10 – 20 mmHg in optimal VAD use[87].

32
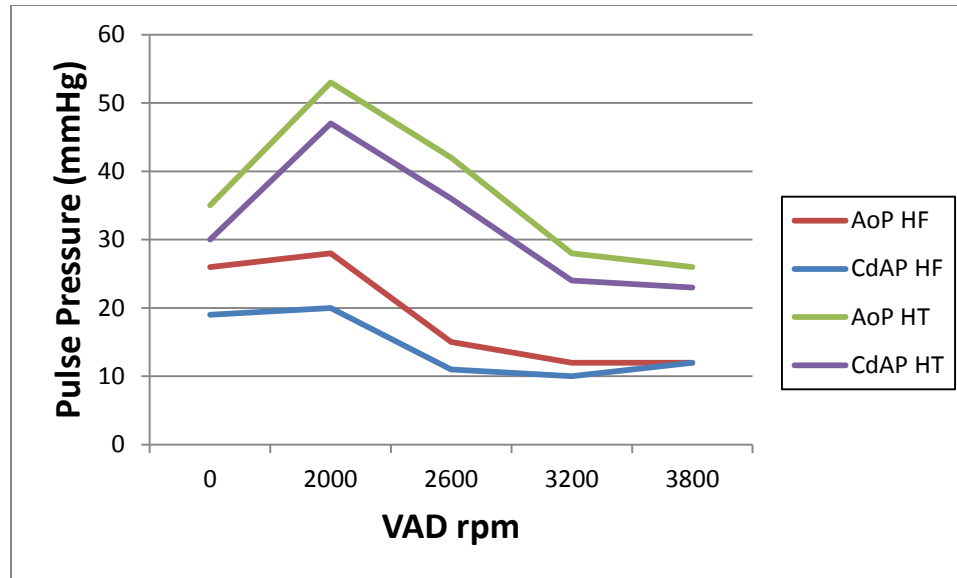
Figure 18. Pulse pressures (mmHg) in incubator testing with increasing CF VAD support

While carotid artery pressures were similar to those from the initial testing, a calibration error led to negative readings for the carotid artery flows. While the flows were negative, they still showed similar amplitude and waveform morphology as those in previous testing. The error was remedied for the final round of testing and proper flows were achieved.

Table 3. Carotid artery pressures and flows in incubator testing versus target values. Values were obtained from figures due to influence of valve ringing in data analysis. Bolded values fall within 10% sensor error range of target values.

Hemodynamic Condition	Target Values				Obtained Values			
	CdAP (mmHg)			CdAF (L/min)	CdAP (mmHg)			CdAF (L/min)
	Systolic	Diastolic	Pulse		Systolic	Diastolic	Pulse	
Normal	100	65	35	0.24 - 0.66	**99**	**69**	30	-0.29
Heart Failure	81	51	30	0.17 - 0.49	**87**	66	21	-0.38
Hypertension	> 117	> 77	40	0.15 - 0.42	**140**	**108**	32	-0.51

33

As one of the primary advantages of this system is its ability to create a multitude of VAD-specific waveforms, a laptop fitted with a VAD pulsatility program was then connected to the system as the VAD controller. Prior to the VAD pulsation data sets, an altered heart failure state was created to match the state established by Ising in previous research[85]. As detailed in the previous section, the VAD was pulsed asynchronously and synchronously at varying time periods and levels of rpm modulation. In the asynchronous mode, unique, yet inconsistent waveforms can be produced when the asynchronous timing produces high degrees of variability in pulse pressure (**Figure 19**). In the synchronous mode, the VAD support drifted from periods of co-pulsation (**Figure 20**) to counter-pulsation (**Figure 21**).
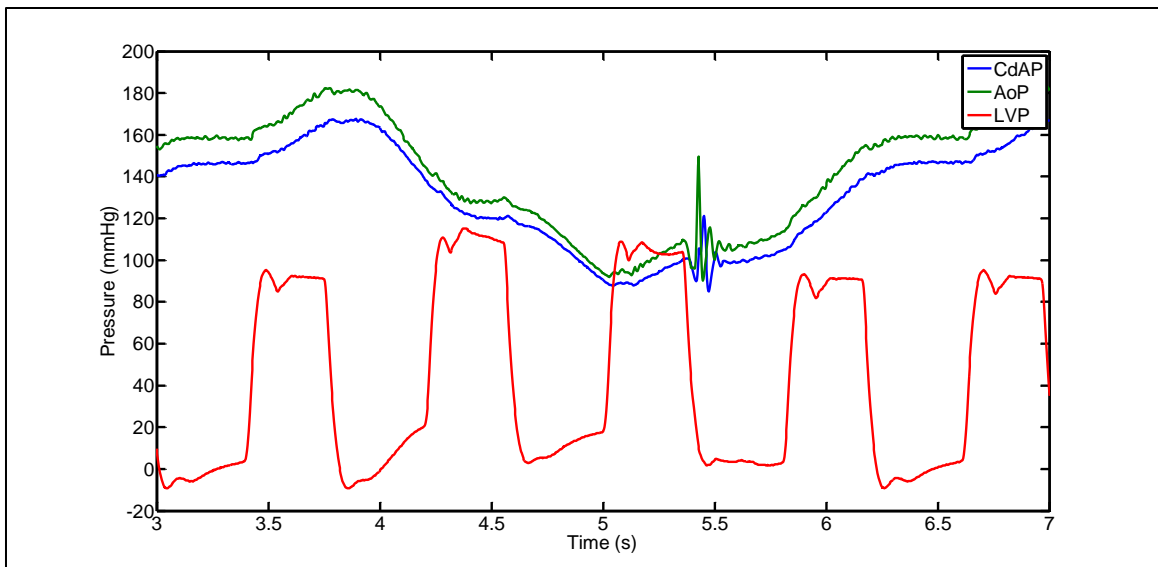
Figure 19. Pressures in asynchronous VAD operation at 3200 +/- 800; cycle time 3.2 seconds
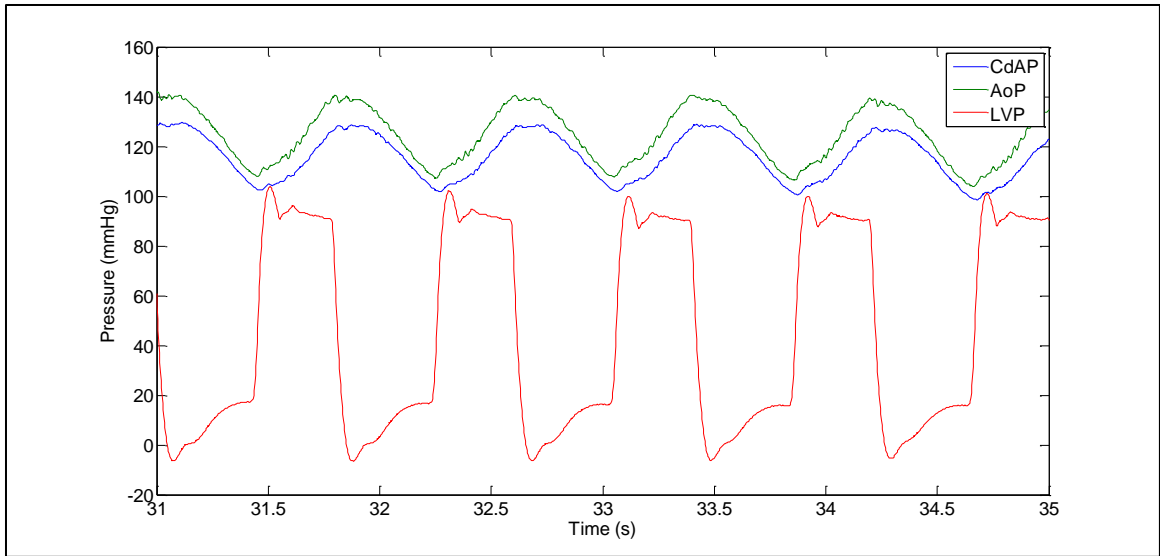
Figure 20. Synchronous co-pulsation at 3200 +/- 800 rpm; cycle time 0.795
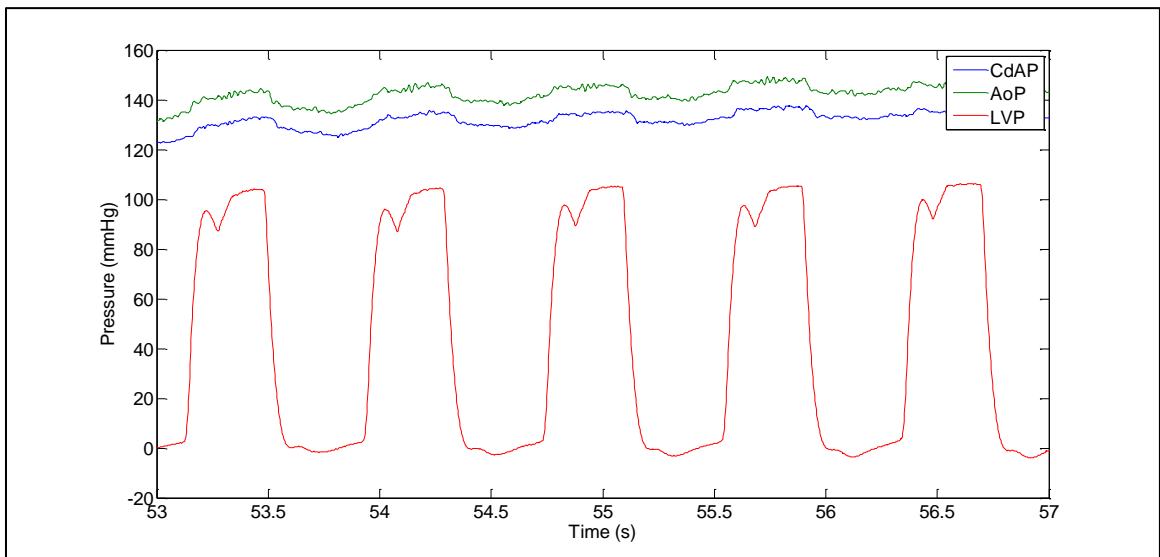
seconds

Figure 21. Synchronous counter-pulsation at 3200 +/- 800 rpm; cycle time

0.795 seconds

In the clinical context, the ultimate goal of these algorithms is to increase

pulsatility in the peripheral vasculature, which can be measured by the

calculation of AoP and CdAP pulse pressures. In the experimental context, these tests were performed to demonstrate that the *ex vivo* system could create complicated VAD-specific hemodynamic waveforms in the presence of a mock left ventricle and with the potential to support artery perfusion. The results in the incubator setup show that, particularly in the synchronous co-pulsation mode of operation, as the 180 degree offset of the pulses in counter-pulsation mode produces destructive interference and results in a near continuous signal. The co-pulsation synchronous mode is able to show near-physiologic aortic pulse pressures, while the counter-pulsation synchronous mode exhibits low aortic pulse pressures. The asynchronous mode of pulsatile VAD flow delivers a variable pulse pressure from beat to beat, which is still greater than pulse pressures provided on full CF VAD support. These compare to a pulse pressure of approximately 10 mmHg at a continuous VAD output of 3200 rpm (**Figure 22**). It should be noted that the low pulse pressure during asynchronous pulsation at 3200 +/- 800 rpm with a pulse width of 0.4 seconds is due to the timing of the pulses, which happened to occur in exact counter-pulsation to the pulses of the ventricle, minimizing pulse pressure as in synchronous counter-pulsation mode.
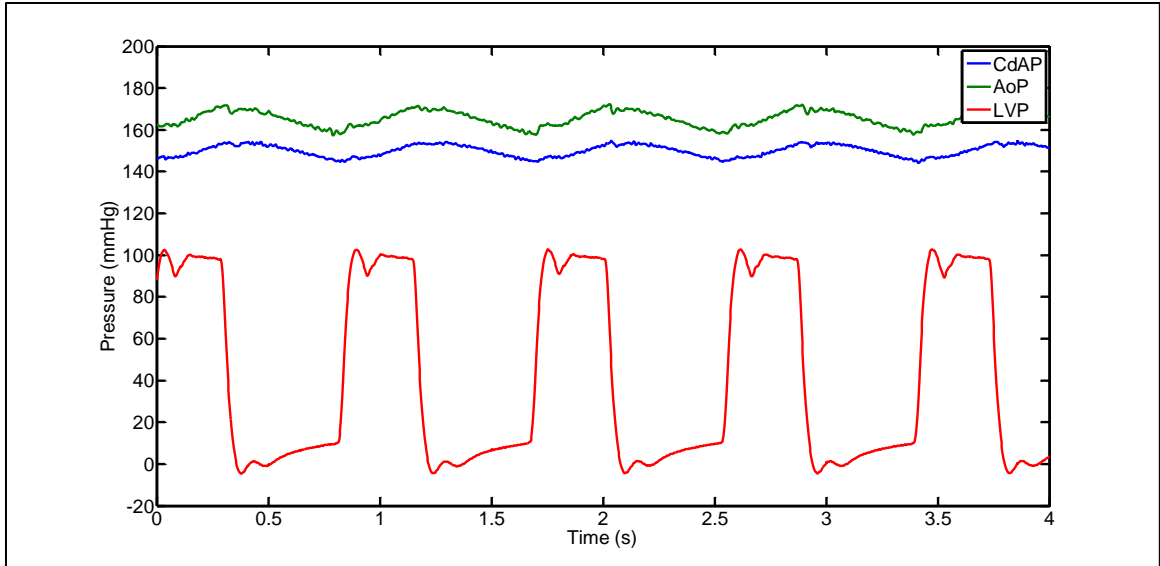
Figure 22. Pressures at full VAD support in Heart Failure condition

Table 4. Pulse pressures in pulsatile mode of VAD operation during incubator

testing

Mode	rpm	Δt	AoP Pulse
Asynchronous	2900 +/- 1100	0.4	36
	2900 +/- 1100	0.5	39
	2900 +/- 1100	0.8	56
	2900 +/- 1100	1.6	102
	3200 +/- 800	0.4	6
	3200 +/- 800	0.5	44
	3200 +/- 800	0.8	50
	3200 +/- 800	1.6	85
Sync Co-pulse	2900 +/- 1100	0.3975	35
	3200 +/- 800	0.3975	33
Sync Counter-pulse	2900 +/- 1100	0.3975	9
	3200 +/- 800	0.3975	9

Baseline normal (**Figure 23**) and heart failure (**Figure 24**) conditions were again established, followed by CF VAD conditions at low, medium, high, and full VAD flow. Trends in flow and pressure in these conditions were normal and matched previous testing results (**Figure 25**).
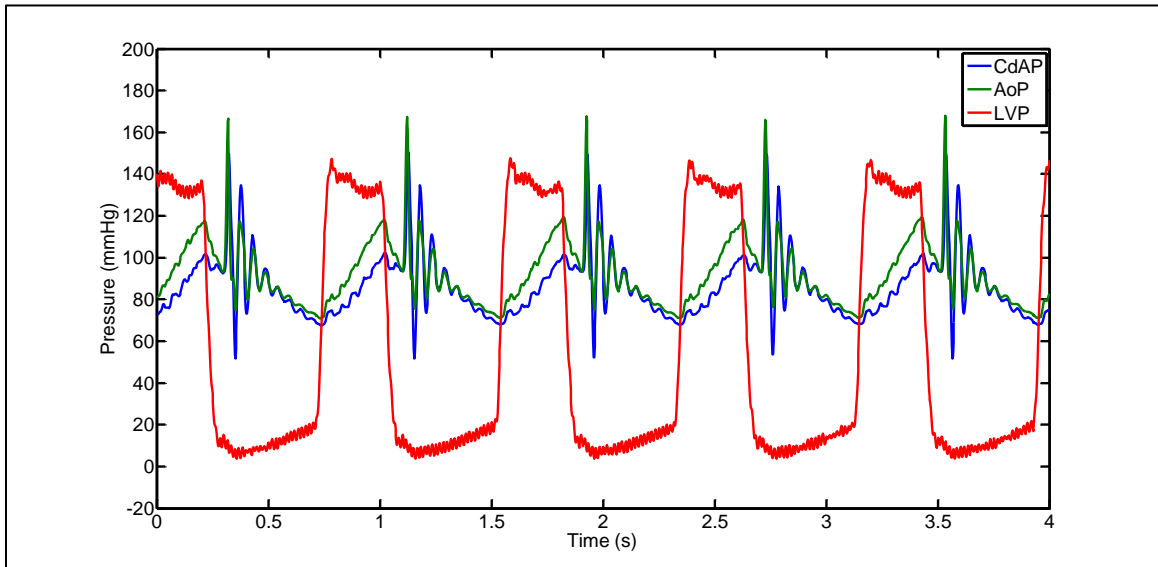
Figure 23. Pressures in normal condition during vessel testing
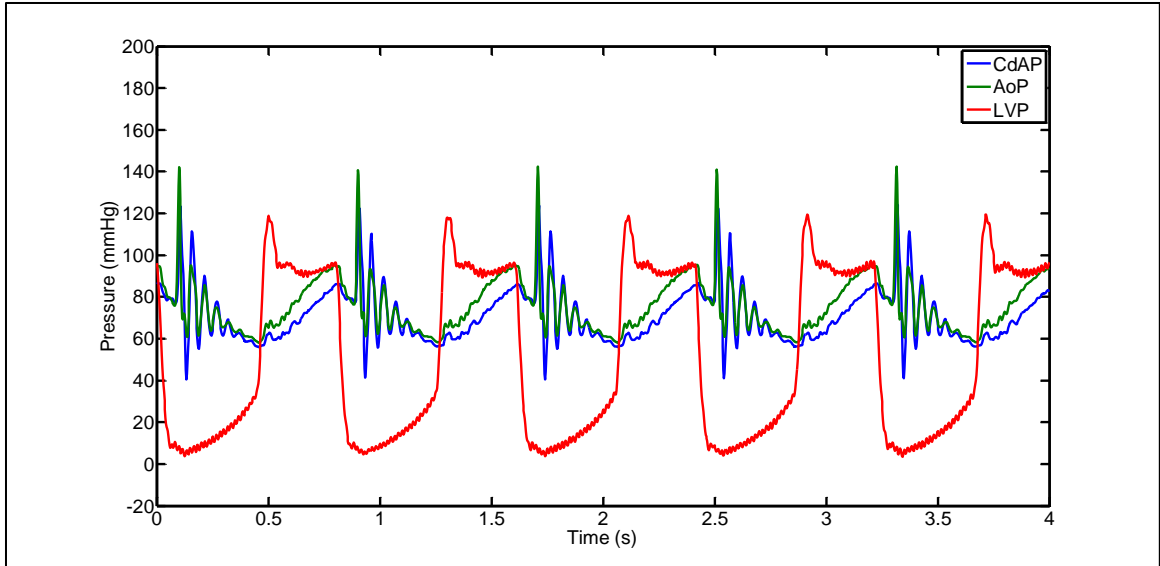
Figure 24. Pressures in heart failure condition during vessel testing
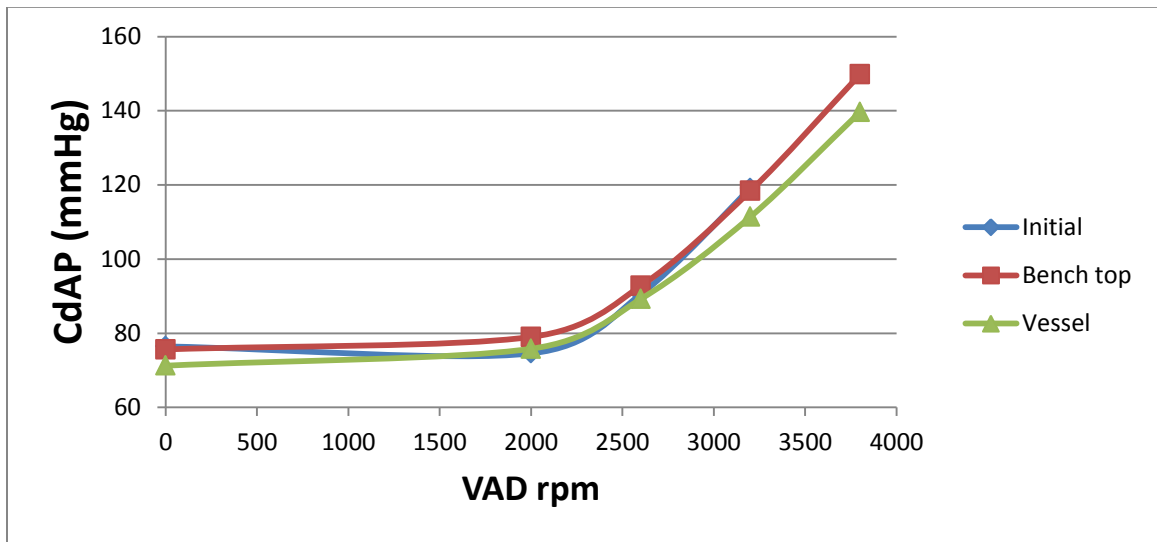
Figure 25. Change in CdAP with increasing VAD flow in heart failure condition

Once those conditions were replicated, data sets of pulsatile VAD flow were taken both asynchronously and synchronously, with both counter-pulsation and co-pulsation being achieved. Pulse pressures in the VAD pulsatility data sets were similar to those previously recorded (**Table 4**), while all carotid artery flows

39

and pressures matched their target values (**Table 5**). All other data from the

vessel testing can be found in **Appendix C**.

Table 5. Carotid artery pressures and flows in vessel testing versus target
values. Values were obtained from figures due to influence of valve ringing in
data analysis. Bolded values fall within 10% sensor error range of target values.

Hemodynamic Condition	Target Values				Obtained Values			
	CdAP (mmHg)			CdAF (L/min)	CdAP (mmHg)			CdAF (L/min)
	Systolic	Diastolic	Pulse		Systolic	Diastolic	Pulse	
Normal	100	65	35	0.24 - 0.66	**102**	**68**	**34**	**0.46**
Heart Failure	81	51	30	0.17 - 0.49	**86**	**56**	**30**	**0.29**

D. <u>Shear Stress Calculations</u>

As previously mentioned, shear stresses in vessels have profound effects on a

wide variety of vascular response mechanisms[71-73, 90-101]. Therefore, shear

stresses were calculated from the obtained volumetric flow measurements, per

the methods utilized by Estrada et al[91]. First, the kinematic viscosity of the fluid

solution used was calculated using equation (**1**):

$$\nu = \frac{\mu}{\rho} \qquad\qquad (1)$$

Normosol-R, a a sterile, nonpyrogenic isotonic solution of balanced electrolytes in

water[102], was used as the fluid solution in order to provide the slight increase in

viscosity over water needed for HVAD operation. Its density was assumed to be

1,010 kg/m³, between the densities of water and blood plasma[103]. Likewise, the

dynamic viscosity was assumed to be 1.10 cP to lie between those of water and blood plasma[104]. Because of their low dynamic viscosities, water and plasma are assumed to be Newtonian fluids whose viscosity is not dependent upon flow rate[105]. Therefore, Normosol-R is also assumed to be a Newtonian fluid. To characterize the flow, the dimensionless Reynold's number was then obtained using equation (**2**):

$$R = \frac{QD_H}{\nu A} \qquad (2)$$

The volumetric flow rate, Q, was attained from the CdAF flow sensor. The hydrodynamic diameter, D_H, for a cylindrical tube is simply the diameter of the tube, and A is the cross-sectional area. The calculation resulted in a value of 1,074, indicating laminar flow. Next, to evaluate the ratio of pulsatile flow frequency to viscous effect, the Wormersly Number was calculated using equation (**3**):

$$\propto = R_H \sqrt{\frac{2\pi f}{\nu}} \qquad (3)$$

The pulsatile frequency, f, was taken as 1.167 Hz for the heart rate of 70 bpm used in most data sets. Similarly to the hydrodynamic diameter, the hydrodynamic radius, R_H, is merely the radius of the tube. A value of 8.238 was obtained, indicating that the pulse frequency is sufficiently low that a parabolic

velocity profile develops during each cycle and is a good approximation to Poiseiulle Flow[91]. Because of this, the shear stress could be estimated using equation (**4**):

$$\tau = \frac{\propto}{\sqrt{2}} \frac{6Q\mu}{2r^3} \qquad\qquad (4)^{91}$$

The radius of the carotid artery channel is represented here as *r*. Using this equation, the shear stresses for each hemodynamic condition were calculated and plotted using Matlab (**Figure 26**).
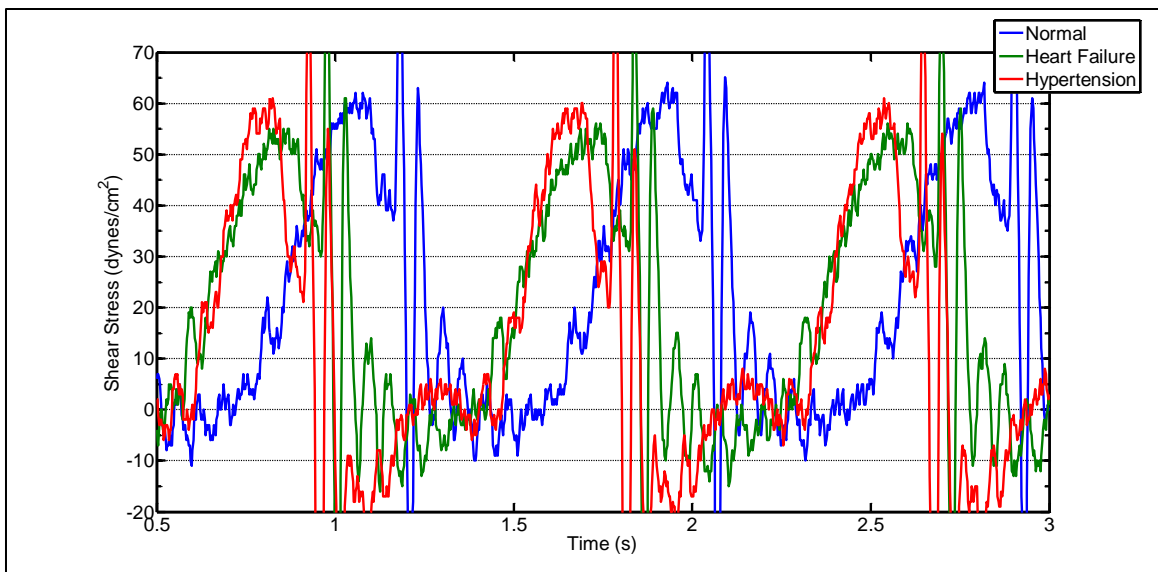
Figure 26. Fluid shear stresses as a function of flow for each hemodynamic condition in initial testing

These shear stresses are slightly higher (~10 dynes/cm^2) than those in previous literature that closely match clinical values[91]. However, they do follow a similar trend where the maximum shear stresses for the normal and heart failure

42

conditions are approximately 5-10 dynes/cm^2 higher than in heart failure.

Average values are not presented, as they are skewed due to the influence of

the mechanical valve ringing.

CHAPTER IV – CONCLUSIONS

A. <u>Limitations</u>

While the system has major advantages over others in literature, it is not without its limitations. First and foremost, there are inherent limitations associated with mock circulatory systems. The mechanical valves cause a ringing effect on the AoP and CdAP, while also having some effect on the LVP waveform. If there effects were considered to be detrimental, the inclusion of tissue valves in the system may remedy some of these effects.

The choice of the incubator for tissue preservation severely constrains the space for the system. However, the majority of the components were able to fit inside. The only exception is the volume reservoir, which required some slight modifications. In the end, the data shows that this limitation was overcome, as the pressure and flow waveforms from the bench top testing were matched in the incubator testing. Expansion of the current system would be difficult given the space constraints of the incubator.

Finally, two limitations specific to the perfusion chamber are vessel loading and throughput. The two unconstrained plungers could cause the vessel to twist and tear in loading, so a more sophisticated loading system is desirable. Also, the single vessel system provides low throughput, although a multiple vessel system is not feasible due to greatly increased complexity to the system and the space constraints previously mentioned.

B. Discussion

Due to limitations of the system, there are some unique features in the data that require explanation. In some instances, the left ventricular pressure drops below zero during diastole. This suction can occur clinically in patients with mitral valve stenosis[106]. As a mechanical valve is rigid, it can behave similarly to a stenosed valve and produce similar suction, depending on the drive pressure of the ventricle. This behavior can also explain the LVP spike in some conditions, as the pressure builds up inside the ventricle momentarily between the time the mitral and aortic valves open. Finally, the ringing cause by the mechanical aortic valve is visible in the pressure waveforms for both AoP and CdAP. While this makes the calculation of pulse pressures more difficult, it otherwise has no effect on the overall results.

While most of the data agrees with known clinical and literature values, some discrepancies do exist. Some pulse pressures and flows are slightly below literature values, which can likely be attributed to operator error. These values can be difficult to attain in real time and are not generated until the full analysis is complete. However, after several rounds of testing and modification, all carotid artery flows and pressures generated fell into their target ranges (**Table 5**), indicating that the system is indeed capable of generating the necessary pressures and flows for the next phase of vessel testing.

Another interesting observation from the results is the behavior of the pulse pressures with increasing VAD flow. The pulse pressures increase slightly with

the introduction of low VAD flow then proceed to drop with increasing VAD flow to below their original levels. An explanation for this trend is that the low VAD flow brings the cardiac output back to a normal level, providing the left ventricle with enough pressure to generate a normal pulse pressure in the arteries. However, as the VAD speed increases and the ventricle is unloaded, this pulse pressure slowly dissipates to levels below the initial value.

One more noteworthy finding from the results is the morphology of the CdAF waveform. While peak and mean CdAF values matched those found in literature, as previously discussed, the resulting waveform was visibly less complex than the referenced waveform (**Figure 27**) [88]. The reasoning behind this is the limited complexity of the system. In the end, the available combinations of resistors and compliance chambers were unable to perfectly recreate the measured waveform and the wave reflections exhibited in a true physiologic circulation. This is most clearly observed when the best fit estimations of both literature and obtained CdAF waveforms were plotted (**Figure 28**). However, with additional testing in the pulsatile VAD, a more accurate waveform may be created due to the ability of the VAD pulsatility to create more complex waveforms (**Figure 29**).
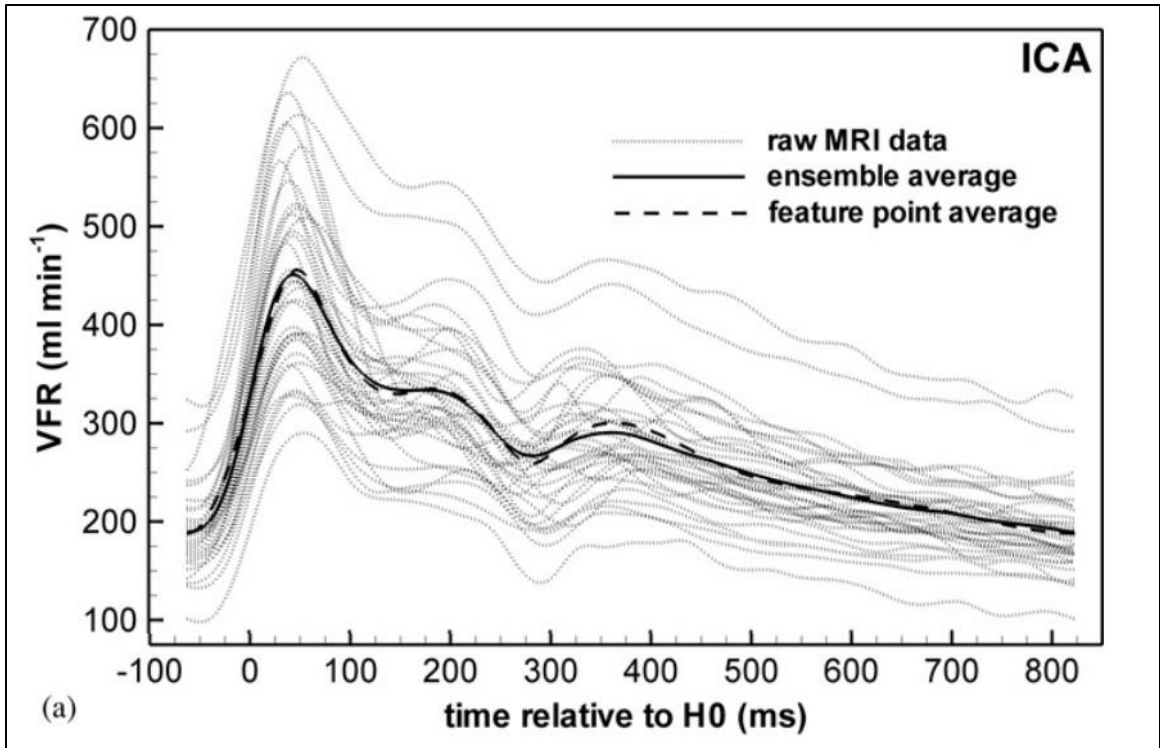
Figure 27. Carotid artery waveform *in vivo* measured via MRI[88]
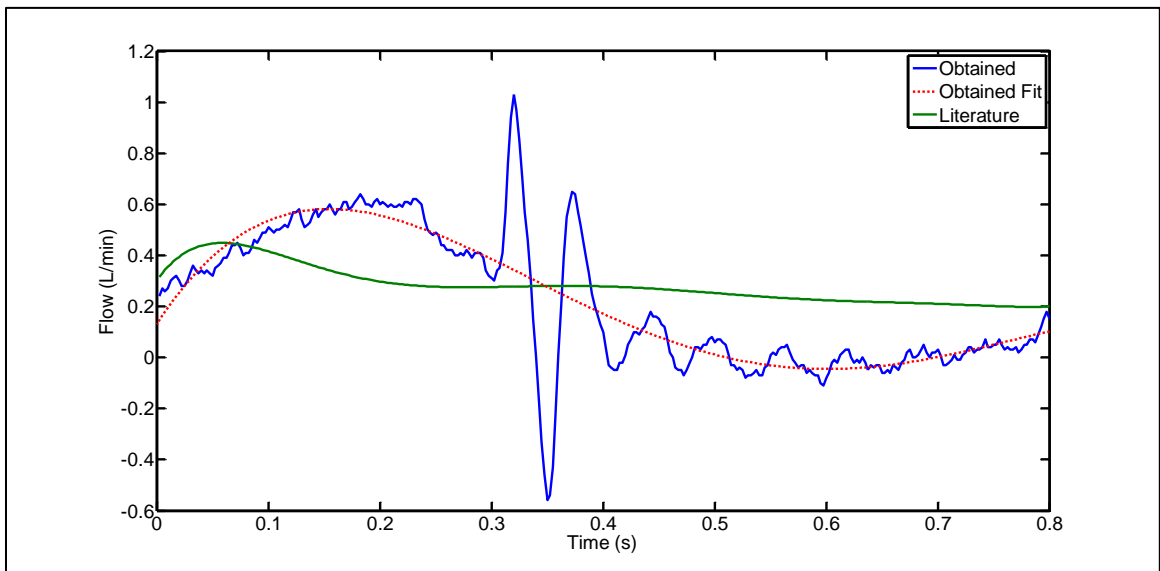
Figure 28. Overlay of obtained CdAF waveform versus estimated polynomial

best fit of literature waveform of CdAF
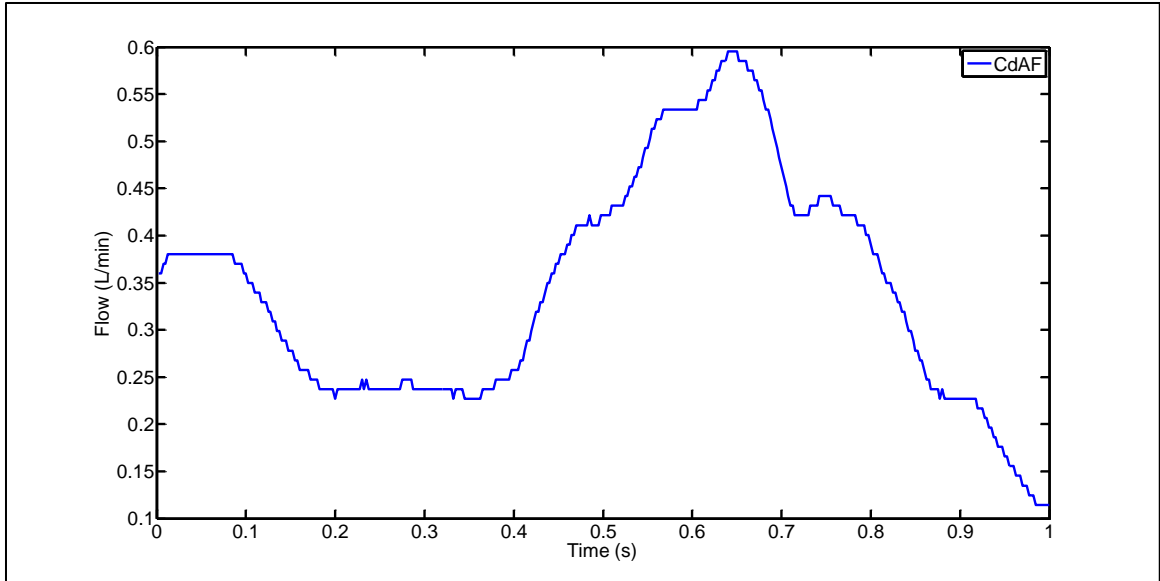
Figure 29. Segment of CdAF waveform in vessel testing during asynchronous

VAD pulsation at 3200 +/- 800 rpm; cycle time 3.2 seconds

In conclusion, the benefits of the system certainly outweigh its limitations. The

hybrid system integrates an *ex vivo* perfusion chamber into a mock circulatory

loop driven by a combination of a mock ventricle and VAD in series. This allows

to system to expose any type of vessel to physiologic, pathologic, and VAD-

specific flows and pressures, a feat that is unprecedented in the current

literature. With the help of future testing, this system will allow for the collection

of valuable data on the vascular response to a wide variety of VAD-specific flow

conditions.

C. Design Improvements

The first and simplest design improvement that could be addressed is

incorporating a thicker plastic tube for the vessel perfusion chamber. For the

current prototype, a 100 mL syringe was used, which has a wall thickness of just under 1/16". This presented an issue when the three screw-in Luer lock ports were inserted into the tubing for fluid exchange and ventilation. The minimal wall thickness required the addition of multiple epoxies and sealants to provide enough material for the ports to screw into. A potential solution would be to use plastic PVC pipe of the same inner diameter, but with an increased thickness of at least 1/8". This would allow the ports to be screwed in to the tubing and create a watertight seal without the use of epoxies and sealants that could potentially have adverse effects on the biocompatibility of the chamber. The placement of these ports could also be adjusted so that the two ports for perfusate circulation are located farther apart to prevent the creation of microcurrents during fluid recirculation.

The main functional flaw with the vessel perfusion chamber prototype was the difficulty in attaching the vessel to the two unconstrained and free moving plungers, then inserting the system into the tube. The possibility existed for the vessel to become twisted or tear, prompting the need for a design that provides a more rigid structure for the cannulated vessel and plungers during reloading into the tube. An additional desired feature was the ability to adjust the length of the vessel inside the chamber. Thus, a screw system similar to that used in a syringe pump (**Figure 30**) was designed. While one plunger remains stationary, the other can be adjusted simply by turning the knob at the end of the threaded rod. O-rings and proper seals should be used to ensure the chamber remained

watertight and the entire system was removable from the tube to allow for proper vessel loading.
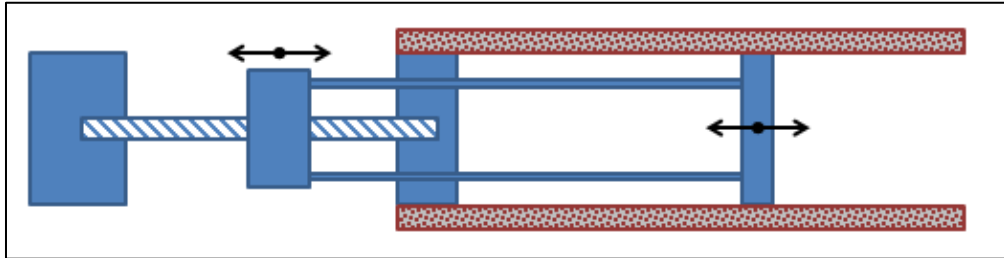
Figure 30. Vessel length adjustment system with components: A. rotating knob, B. traveling screw element, C. fixed plunger, D. sliding plunger

Another design improvement would be to address one of the main constraints of the incubator setup: the inability to properly adjust the height of the fluid reservoir. This controls the preload and has a direct effect on the left ventricular end-diastolic pressure. The lack of adjustability is due to the reservoir being contained on the top shelf of the incubator, which is set at a maximum height due to the height of the two compliance chambers below. However, a vacant space exists below the top shelf and above the mock ventricle to the side of the compliance chambers. A potential solution to allow some degree of preload adjustment is to create a secondary shelf that attaches to the top incubator shelf. The shelf would be half the width of the main incubator shelves so as not to interfere with the compliance chambers, and would be suspended from the upper shelf by four metal rods that would rise up through the holes in the metal

shelf. The height of the shelf would be adjustable by knobs at the end of each rod, thus allowing for the maximal degree of preload adjustability.

D. <u>Future Testing</u>

This *ex vivo* vessel perfusion system lays the foundation for a tremendous amount of testing on bovine carotid arteries utilizing complex hemodynamic and VAD-specific waveforms. These proposed studies will test the hypothesis that diminished pulsatility produced by CF VAD adversely alters vascular function and remodeling, which may contribute to the observed clinical complications, as well as limit the potential for myocardial recovery. If substantiated experimentally in these studies, flow modulation by varying pump speed (rpm) may provide a viable solution. To test this hypothesis, two specific aims will be completed. The first specific aim is to quantify the vascular function of carotid arteries and aorta from healthy and heart failure (HF) bovine models in a mock circulation system with *ex vivo* perfusion for 72 hours and compare aortic gene expression to human HF patients. These experiments will utilize the *ex vivo* vessel perfusion system to demonstrate that *ex vivo* bovine carotid arteries and aortas remain viable for up to 72 hours with simulated physiologic flows. Tissue viability will be measured using hematoxylin and eosin (H&E) staining and methyl thiazole tetrazolium (MTT) assays. Arterial contractility, endothelial function, and mechanical properties will be quantified for normal and HF animals. This will be accomplished by using flow-mediated dilation techniques, examining pressure-

diameter-thickness relationships, performing calculations of compliance, using vascular tension assays, and comparing clinical gene expression.

Finally, the second specific aim will test the hypothesis that increased vascular pulsatility by flow modulation of rotary blood pumps can restore vascular phenotype, structure, and function using the *ex vivo* perfusion system. This aim will measure arterial responses to CF VAD flow modulation, including vasoconstriction, endothelial function, and arterial remodeling via methods previously described in the first two specific aims. Testing will again be performed at three VAD speeds in addition to various levels of flow modulation using the aforementioned VAD pulsatility program.

The long-term objective of this testing is to continue to improve HF patient outcomes and quality of life by developing safe and effective mechanical support strategies for ventricular unloading as well as peripheral targets of the integrated HF condition. While much testing still needs to be performed, the creation of the *ex vivo* vessel perfusion system is the first step in the process. The system's ability to create hemodynamically complex, VAD-specific waveforms via the combination of the mock ventricle and VAD in series in three different hemodynamic conditions, while still being small enough to fit in the incubator lays a foundation for years of clinically-relevant future experimentation, specifically on the influence of pulsatile versus continuous VAD-generated flow on the arteries.

	000	001	002	003	004	005	006	007	008	009	010	011	012	013	
	no VAD	lo VAD	med VAD	med VAD	hi VAD	HT; no VAD	HT; lo VAD	HT; med VAD	HT; hi VAD	normal	HF	HF; lo VAD	HF; med VAD	HF; hi VAD	
LVHR	69.773	69.72	69.702	69.726	69.714	69.708	69.702	69.714	69.726	69.712	69.753	69.877	70.024	69.745	LVHR
LVSV	58.875	35.268	11.39	18.477	-0.000337	47.27	31.66	14.472	0.60078	59.145	52.542	26.401	6.9525	0	LVSV
LVCO	4.1079	2.4589	0.79392	1.2883	-2.35E-05	3.2951	2.2068	1.0089	0.041889	4.1231	3.6649	1.8449	0.48665	0	LVCO
LVPbd	-7.1064	-10.04	-15.613	-14.52	-17.352	-6.2209	-4.634	-5.607	-7.558	-11.776	-4.1395	-13.292	-15.767	-19.149	LVPbd
LVPed	10.063	8.6766	1.9086	4.0903	-2.3246	3.0857	6.5609	6.6668	5.5882	3.2005	13.913	5.4904	4.0175	0.09852	LVPed
LVPpksys	141.91	137.25	136.27	135.22	142.33	171.94	169.55	178.59	183.69	145.28	130.99	124.94	123.75	119.93	LVPpksys
LVppdPdt	3763.5	3545.8	3252.4	3328.8	3125.9	3822.4	3852.1	3854.7	3841.2	3624.3	3774.9	3567.5	3473	3297.4	LVppdPdt
LVpndPdt	-3207.4	-3161.8	-3034.8	-3061.9	-3173.9	-3551.5	-3444.6	-3529.1	-3730.9	-3200.9	-3196.7	-3130.3	-3161.7	-3185.1	LVpndPdt
LVEd	0.29162	0.53071	1.5385	1.0073	-16123	0.19689	0.3536	0.84814	22.544	0.25322	0.34359	0.7114	2.8456	NaN	LVEd
LVEW	7283.7	4378.1	1569.2	2456.6	-0.20624	7736.1	4933.6	2380.6	100.8	7998.9	5687.1	2888.8	813.6	-0.33714	LVEW
AoPavg	94.983	86.91	107.87	100.15	126.62	129.93	122.48	140.12	163.45	97.507	81.652	80.41	96.138	125.78	AoPavg
AoPpulse	97.484	75.3	58.544	66.1	22.691	100.03	91.902	76.28	48.364	85.001	80.969	67.131	45.548	21.796	AoPpulse
AoPsys	170.28	142.03	151.7	149.38	138.86	203.43	180.46	186.53	186.93	165.43	147.34	130.36	128.84	137.86	AoPsys
AoPdia	72.799	66.734	93.153	83.278	116.17	103.4	88.557	110.25	138.56	80.431	66.374	63.225	83.291	116.07	AoPdia
AoFavg	3.8071	2.1573	0.45424	0.96278	-0.30741	2.9716	1.8947	0.68448	-0.35916	3.8201	3.3983	1.5792	0.19178	-0.32917	AoFavg
AoFpulse	19.701	15.922	8.9897	11.25	0.505	17.813	15.759	10.503	2.2482	19.956	17.747	13.192	7.277	0.46559	AoFpulse
AoFpkpos	12.988	9.2362	3.3679	5.1829	-0.0055882	10.941	9.2012	5.3291	0.61294	13.312	11.24	7.0727	2.8145	-0.065588	AoFpkpos
AoFpkneg	-6.7132	-6.6856	-5.6218	-6.0674	-0.51059	-6.8724	-6.5574	-5.1735	-1.6353	-6.6436	-6.5065	-6.1194	-4.4624	-0.53118	AoFpkneg
TPRc	1997.8	3223.5	19008	3223.4	-32955	3498.1	5172.2	16381	-36424	2042.2	1922.4	4080.6	40829	-30572	TPRc
CdAPavg	84.623	81.307	102.46	94.715	120.95	125.25	117.37	135.33	159	91.335	76.452	74.574	90.515	119.14	CdAPavg
CdAPmax	153.6	136.45	145.9	144.19	129.78	196.68	180.67	181.77	179.9	154.66	138.4	126.35	120.62	127.78	CdAPmax
CdAPmin	64.929	43.308	70.051	59.462	111.83	93.573	86.796	108.58	136.25	64.375	48.316	36.869	65.563	110.96	CdAPmin
LVPavg	52.237	47.348	45.304	45.62	44.168	65.306	65.828	68.695	69.646	51.34	44.621	44.32	43.666	39.873	LVPavg
LVPmax	141.91	137.25	136.27	135.22	142.33	171.94	169.55	178.59	183.69	145.28	130.99	124.94	123.75	119.93	LVPmax
LVPmin	-7.121	-10.048	-15.65	-14.562	-17.367	-7.3634	-4.6495	-5.6315	-7.572	-12.29	-8.5811	-13.314	-15.797	-19.167	LVPmin
CdAFpkpos	0.20109	0.17437	0.19839	0.1884	0.23998	0.11827	0.077484	0.094598	0.12613	0.21735	0.18146	0.19146	0.21756	0.28319	CdAFpkpos
CdAFpkneg	0.98147	0.85765	0.89147	0.92794	0.45794	0.99941	0.88353	0.78912	0.56735	1.0079	0.92	0.89727	0.7403	0.51794	CdAFpkneg
CdAFpulse	-0.65382	-0.32118	-0.24824	-0.28029	0.054706	-0.90412	-0.54118	-0.31676	-0.17559	-0.5303	-0.57176	-0.31818	-0.072727	0.084412	CdAFpkneg
CdAFpulse	1.6353	1.1788	1.1397	1.2082	0.40324	1.9035	1.4247	1.1059	0.74294	1.5382	1.4918	1.2155	0.81303	0.43353	CdAFpulse
LVDFavg	0	1.4859	4.1029	3.2805	5.4397	-0.030975	0.59944	2.1815	3.5804	-0.030074	-0.03107	1.9565	3.9889	5.4051	LVDFavg
LVDFpkpos	0	6.8129	9.5532	8.7674	10.769	0.0073529	6.7397	8.6929	10.639	0.11909	0.10941	6.5991	8.7236	9.6521	LVDFpkpos
LVDFpkneg	0	-2.2124	0.18353	-0.74941	1.7518	-0.071176	-3.9347	-2.6115	-1.6624	-0.18909	-0.18912	-1.7509	0.21394	2.0841	LVDFpkneg
LVDFpulse	0	9.0253	9.3697	9.5168	9.0174	0.078529	10.674	11.304	12.301	0.30818	0.29853	8.35	8.5097	7.5679	LVDFpulse

APPENDIX B – INCUBATOR TESTING DATA

	001	002	004	005	006	007	008	009	010	011	012	013	014	015	016	017	018
	baseline	lo VAD	full VAD	baseline	HF, no VAD	HF, lo VAD	HF, med VAD	HF, hi VAD	HF, full VAD	HT, no VAD	HT, lo VAD	HT, med VAD	HT, hi VAD	HT, full VAD	baseline	HF, no VAD	adjusted HF
LVHR	69.673	69.717	69.717	59.765	69.708	69.717	69.704	69.72	69.717	69.717	69.717	69.73	69.704	69.72	69.72	59.765	75.652
LVSV	71.046	51.301	0	77.49	51.324	28.738	4.5948	0	0	57.325	48.28	28.365	5.7103	0	64.815	56.856	45.525
LVCO	4.95	3.5766	0	4.6312	3.5777	2.0035	0.32028	0	0	3.9965	3.366	1.9779	0.39803	0	4.5189	3.398	3.444
LVPbd	5.611	4.6914	-10.25	10.925	9.7863	10.053	3.2767	-0.51834	-4.547	11.98	5.3966	2.7087	1.3203	-0.50478	7.7588	13.531	12.158
LVPed	13.429	15.611	1.3585	20.663	25.212	26.631	22.752	16.644	11.266	27.418	31.343	29.781	28.734	21.71	30.84	30.84	18.102
LVPpksys	140.33	137.7	139.69	137.24	116.05	114.11	112.33	108.02	102.62	167.27	157.2	161.91	167.48	165.35	142.35	114.17	108.08
LVpppPdt	3293.7	3277.6	2736.5	3354.1	2902.6	2840.6	2755.6	2634	2455.9	3753	3759.5	3712.6	3688.5	3597.4	3702.6	2863.9	2487
LVpndPdt	-2950.5	-2876.9	-2715.9	-2836.9	-2610.3	-2545.7	-2583.7	-2589	-2398.9	-3385.6	-3208.5	-3284.3	-3368.1	-3210.9	-3467	-2583.7	-2277.9
LVEd	0.11006	0.21287	NaN	0.12567	0.30055	0.57691	4.2408	NaN	NaN	0.26944	0.53743	0.9545	4.8064	NaN	0.21525	0.30441	0.13234
LVEW	7763.1	5508.5	-0.79334	8306.2	3993.9	2304.6	430.22	-0.47756	-0.98436	7688.5	5966.8	3822	-1.2574	6995.6	4481.6	3702.6	3702.6
AoPavg	94.757	93.902	153.56	94.616	81.092	85.107	100.55	129.54	165.12	128.96	133.23	152.58	192.69	196.04	95.324	79.912	82.796
AoPpulse	100.09	88.352	17.814	102.92	84.334	73.203	49.437	14.472	14.062	105.21	99.594	91.476	67.249	26.937	101.56	92.609	111.36
AoPsys	177.59	160.28	162.35	178.34	153.23	143.55	141.06	136.44	172.11	217.94	190.69	202.77	203.99	205.14	178.66	156.36	160.96
AoPdia	77.501	71.933	144.53	75.416	68.894	70.35	91.62	121.97	158.05	112.73	91.096	111.3	136.74	178.2	77.101	63.751	49.593
AoFavg	4.515	3.1442	-0.37358	4.2462	3.1752	1.6456	0.0039128	-0.29625	-0.39182	3.5343	2.9436	1.5198	-0.069166	-0.45323	4.0975	3.0672	3.0527
AoFpulse	22.832	19.043	0.40125	21.168	17.66	12.912	4.6681	0.30882	0.25812	20.156	18.722	13.784	6.3187	0.44412	20.912	17.496	15.961
AoFpkpos	16.785	13.236	-0.13563	15.098	11.907	7.795	1.605	-0.12235	-0.2525	13.73	13.031	8.4544	2.3706	-0.19824	14.702	12.01	10.522
AoFpkneg	-6.0476	-5.8069	-0.53688	-6.07	-5.7529	-5.1169	-3.0631	-0.43118	-0.51063	-6.4256	-5.6913	-5.3294	-3.9481	-0.64235	-6.2106	-5.4864	-5.4385
TPRc	1679.4	2389.5	-32895	1782.9	2043.6	4138.9	8.31E+05	-35018	-33757	2919.7	3197.9	7019.2	-2.80E+05	-34023	1861.5	2084.8	2188.5
CdAPavg	86.147	85.765	137.96	84.903	75.64	79.003	92.746	118.38	149.78	123.75	112.85	127.77	146.27	184.35	87.737	74.836	77.274
CdAPmax	125.09	120.43	144	121.9	110.07	106.27	110.51	123.09	154.3	185.83	178.95	181.92	196.04	196.04	114.78	121.5	114.78
CdAPmin	61.11	68.072	131.22	65.505	53.931	60.256	80.885	112.87	144.57	108.9	167.22	108.54	131.98	171.78	69.626	61.564	57.285
LVPavg	53.351	52.138	47.68	56.679	49.567	48.548	49.136	45.505	40.624	72.457	70.908	72.883	69.669	57.378	50.667	49.866	49.866
LVPmax	140.33	137.7	139.69	137.24	116.05	114.11	112.33	108.02	102.62	167.27	157.2	161.91	167.48	165.35	142.35	114.17	108.08
LVPmin	-0.42816	-1.2986	-10.268	0.90951	6.8116	5.5024	3.2517	-5.4074	-4.5708	6.4349	2.6805	1.3078	-0.5207	2.0332	7.0582	3.8796	3.8796
CdAFavg	-0.1353	-0.1503	0.085447	-0.29474	-0.38229	-0.37048	-0.33552	-0.26385	-0.18927	-0.51106	-0.50362	-0.48279	-0.43922	-0.24062	-0.45756	-0.41371	-0.41371
CdAFpkpos	0.085478	0.078923	0.1528	-0.055051	-0.19499	-0.18652	-0.19529	-0.20383	-0.13393	-0.34679	-0.36557	-0.33302	-0.34992	-0.39533	0.077818	-0.2561	-0.21451
CdAFpkneg	-0.3423	-0.32488	0.018197	-0.47218	-0.56207	-0.52897	-0.42066	-0.32049	-0.23723	-0.74245	-0.75059	-0.7293	-0.65293	-0.47841	-0.47192	-0.6167	-0.56645
CdAFpulse	0.42777	0.4038	0.1346	0.41713	0.36708	0.34245	0.22538	0.11667	0.1033	0.39566	0.38502	0.39629	0.30301	0.08308	0.54974	0.3606	0.35194
LVDFavg	-0.32348	0.95812	6.5082	-0.31757	-0.31871	1.3329	3.5265	4.5991	5.4903	-0.29875	0.054678	1.7909	3.7855	4.8927	-0.32009	-0.32222	-0.32062
LVDFpkpos	-0.29	6.245	10.395	-0.28286	-0.28882	5.6394	7.4475	8.0182	8.3644	-0.2675	5.9888	7.8019	9.8125	10.406	-0.29294	-0.28786	-0.29189
LVDFpkneg	-0.35471	-2.8138	3.8431	-0.35214	-0.34941	-1.915	0.6475	2.0688	3.3013	-0.33063	-4.2244	-2.7906	-0.79625	0.81059	-0.35	-0.35071	-0.34689
LVDFpulse	0.064706	9.0587	6.5519	0.069286	0.060588	7.5544	6.8	5.9494	5.0631	0.063125	10.213	10.592	10.609	9.5953	0.057059	0.062857	0.055

APPENDIX C – VESSEL TESTING DATA

	002	003	004	005	006	007	
	baseline	modified HF	HF, lo VAD	HF, med VAD	HF, hi VAD	HF, full VAD	
LVHR	74.672	74.703	74.734	74.679	74.691	74.686	LVHR
LVSV	69.233	53.301	27.455	4.9203	0.00061392	0	LVSV
LVCO	5.1697	3.9817	2.0518	0.36745	4.60E-05	0	LVCO
LVPbd	14.663	11.776	38.08	36.034	34.246	31.908	LVPbd
LVPed	21.063	36.109	20.108	29.645	29.355	19.479	LVPed
LVPpksys	146.81	119.7	134.66	131.52	128.52	121.56	LVPpksys
LVppdPdt	4048.9	3422.7	9829	9401.2	9617.7	9269.1	LVppdPdt
LVpndPdt	-3743.1	-3203.3	-9492.7	-9356.2	-9498.6	-9490.6	LVpndPdt
LVEd	0.092439	0.45639	0.1236	1.7087	207.14	NaN	LVEd
LVEW	7470.4	3964.8	2130.8	428.35	-0.17921	-0.92132	LVEW
AoPavg	92.155	75.991	81.262	94.963	118.49	148.5	AoPavg
AoPpulse	96.043	83.169	72.974	32.207	18.026	16.662	AoPpulse
AoPsys	167.11	141.32	134.99	115.84	127.69	157.06	AoPsys
AoPdia	71.065	58.152	62.013	83.634	109.66	140.4	AoPdia
AoFavg	4.8139	3.6885	1.7599	0.056954	-0.32597	-0.43026	AoFavg
AoFpulse	23.405	17.111	11.851	3.4949	0.48393	0.37386	AoFpulse
AoFpkpos	18.415	12.608	7.8923	2.0376	-0.05578	-0.22685	AoFpkpos
AoFpkneg	-4.9897	-4.5032	-3.9592	-1.4573	-0.53971	-0.60071	AoFpkneg
TPRc	1531.7	1648.8	3697.9	1.39E+05	-29162	-27712	TPRc
CdAPavg	86.329	71.252	75.811	89.237	111.39	139.63	CdAPavg
CdAPmax	149.79	123.35	111.99	104.23	119.24	146.58	CdAPmax
CdAPmin	52.244	41.108	53.612	80.144	103.77	132.88	CdAPmin
LVPavg	57.095	51.451	50.462	50.782	47.435	42.231	LVPavg
LVPmax	146.81	119.7	127.17	131.52	128.52	121.56	LVPmax
LVPmin	4.009	3.1183	-19.922	-22.145	-25.517	-28.72	LVPmin
CdAFavg	0.4558	0.29041	0.32644	0.34437	0.33255	0.46865	CdAFavg
CdAFpkpos	1.045	0.67858	0.79536	0.57406	0.46783	0.65522	CdAFpkpos
CdAFpkneg	0.079613	0.02929	0.072997	0.18039	0.20823	0.30817	CdAFpkneg
CdAFpulse	0.96536	0.64929	0.72237	0.39366	0.2596	0.34705	CdAFpulse

CHAPTER V – REFERENCES

1. High blood pressure (hypertension). *Mayo Clinic*. 2010
2. Giridharan GA, Ewert DL, Pantalos GM, Gillars KJ, Litwak KN, Gray LA, Koenig SC. Left ventricular and myocardial perfusion responses to volume unloading and afterload reduction in a computer simulation. *Asaio J*. 2004;50:512-518
3. Marshall I, Papathanasopoulou P, Wartolowska K. Carotid flow rates and flow division at the bifurcation in healthy volunteers. *Physiological Measurement*. 2004;25:691
4. Holdsworth D, Norley C, Frayne R, Steinman D, Rutt B. Characterization of common carotid artery blood-flow waveforms in normal human subjects. *Physiological Measurement*. 1999;20:219
5. Morgan AJ, Hosking SL. Non-invasive vascular impedance measures demonstrate ocular vasoconstriction during isometric exercise. *British journal of ophthalmology*. 2007;91:385
6. Go AS, Mozaffarian D, Roger VL, Benjamin EJ, Berry JD, Borden WB, Bravata DM, Dai SF, Ford ES, Fox CS, Franco S, Fullerton HJ, Gillespie C, Hailpern SM, Heit JA, Howard VJ, Huffman MD, Kissela BM, Kittner SJ, Lackland DT, Lichtman JH, Lisabeth LD, Magid D, Marcus GM, Marelli A, Matchar DB, McGuire DK, Mohler ER, Moy CS, Mussolino ME, Nichol G, Paynter NP, Schreiner PJ, Sorlie PD, Stein J, Turan TN, Virani SS, Wong ND, Woo D, Turner MB, Amer Heart A, Stroke Stat S. Heart disease and stroke statistics-2013 update a report from the american heart association. *Circulation*. 2013;127:E6-E245
7. Khazanie P, Rogers JG. Patient selection for left ventricular assist devices. *Congestive heart failure (Greenwich, Conn.)*. 2011;17:227-234
8. Heart failure - overview. *PubMed Health*. 2013
9. Klabunde RE. Pathophysiology of heart failure. *Cardiovascular Physiology Concepts*. 2007;2013
10. Overgaard CB, Džavík V. Inotropes and vasopressors: Review of physiology and clinical use in cardiovascular disease. *Circulation*. 2008;118:1047-1056
11. Kato TS, Chokshi A, Singh P, Khawaja T, Cheema F, Akashi H, Shahzad K, Iwata S, Homma S, Takayama H, Naka Y, Jorde U, Farr M, Mancini DM, Schulze PC. Effects of continuous-flow versus pulsatile-flow left ventricular assist devices on myocardial unloading and remodeling. *Circulation: Heart Failure*. 2011;4:546-553
12. Li M, Scott DE, Shandas R, Stenmark KR, Tan W. High pulsatility flow induces adhesion molecule and cytokine mrna expression in distal pulmonary artery endothelial cells. *Ann. Biomed. Eng.* 2009;37:1082-1092
13. Orime Y, Shiono M, Hata H, Yagi S, Tsukamoto S, Okumura H, Nakata K, Kimura S, Hata M, Sezai A, Sezai Y. Cytokine and endothelial damage in pulsatile and nonpulsatile cardiopulmonary bypass. *Artif. Organs*. 1999;23:508-512

14. Torre-Amione G, Stetson SJ, Youker KA, Durand JB, Radovancevic B, Delgado RM, Frazier OH, Entman ML, Noon GP. Decreased expression of tumor necrosis factor-alpha in failing human myocardium after mechanical circulatory support - a potential mechanism for cardiac recovery. *Circulation.* 1999;100:1189-1193

15. James JEA, Daly MDB. Comparison of reflex vasomotor responses to separate and combined stimulation of carotid sinus and aortic arch baroreceptors by pulsatile and non-pulsatile pressures in dog. *J. Physiol.-London.* 1970;209:257-&

16. Munakata M, Imai Y, Takagi H, Nakao M, Yamamoto M, Abe K. Altered frequency-dependent characteristics of the cardiac baroreflex in essential-hypertension. *J. Auton. Nerv. Syst.* 1994;49:33-45

17. Nakano T, Tominaga R, Nagano I, Okabe H, Yasui H. Pulsatile flow enhances endothelium-derived nitric oxide release in the peripheral vasculature. *Am. J. Physiol.-Heart Circul. Physiol.* 2000;278:H1098-H1104

18. Haga JH, Li YSJ, Chien S. Molecular basis of the effects of mechanical stretch on vascular smooth muscle cells. *J. Biomech.* 2007;40:947-960

19. Stoner L, Young JM, Fryer S, Sabatier MJ. The importance of velocity acceleration to flow-mediated dilation. *International journal of vascular medicine.* 2012;2012:589213

20. Habazettl H, Kukucka M, Weng YG, Kuebler WM, Hetzer R, Kuppe H, Pries AR. Arteriolar blood flow pulsatility in a patient before and after implantation of an axial flow pump. *Ann. Thorac. Surg.* 2006;81:1109-1111

21. Vasku J, Wotke J, Dobsak P, Baba A, Rejthar A, Kuchtickova S, Imachi K, Abe Y, Saito I, Isoyama T, Nitta S-I, Yambe T. Acute and chronic consequences of non-pulsatile blood flow pattern in long-term total artificial heart experiment. *Pathophysiology : the official journal of the International Society for Pathophysiology / ISP.* 2007;14:87-95

22. Undar A, Masai T, Beyer EA, Goddard-Finegold J, McGarry MC, Fraser CD. Pediatric physiologic pulsatile pump enhances cerebral and renal blood flow during and after cardiopulmonary bypass. *Artif. Organs.* 2002;26:919-923

23. Saito S, Westaby S, Piggot D, Dudnikov S, Robson D, Catarino PA, Clelland C, Nojiri C. End-organ function during chronic nonpulsatile circulation. *Ann. Thorac. Surg.* 2002;74:1080-1085

24. Hornick P, Taylor K. Pulsatile and nonpulsatile perfusion: The continuing controversy. *J. Cardiothorac. Vasc. Anesth.* 1997;11:310-315

25. Wang W, Bai SY, Zhang HB, Bai J, Zhang SJ, Zhu DM. Pulsatile flow improves cerebral blood flow in pediatric cardiopulmonary bypass. *Artif. Organs.* 2010;34:874-878

26. Slaughter MS. Hematologic effects of continuous flow left ventricular assist devices. *J. Cardiovasc. Transl. Res.* 2010;3:618-624

27. Yozu R, Golding L, Yada I, Harasaki H, Takatani S, Kawada S, Nosé Y. Do we really need pulse? Chronic nonpulsatile and pulsatile blood flow: From the exercise response viewpoints. *Artif. Organs.* 1994;18:638-642

28. Gao B, Chang Y, Gu KY, Zeng Y, Liu YJ. A pulsatile control algorithm of continuous-flow pump for heart recovery. *Asaio J.* 2012;58:343-352

29. Colacino FM, Arabia M, Moscato F, Danieli GA. Modeling, analysis, and validation of a pneumatically driven left ventricle for use in mock circulatory systems. *Medical engineering & physics.* 2007;29:829-839

30. Taylor CE, Miller GE. Mock circulatory loop compliance chamber employing a novel real-time control process. *J. Med. Devices.* 2012;6

31. Taylor CE, Miller GE. Implementation of an automated peripheral resistance device in a mock circulatory loop with characterization of performance values using simulink simscape and parameter estimation. *J. Med. Devices.* 2012;6

32. Cheng SJ, Hsu PL, McMahon RA. A hybrid mock circulatory system for cardiovascular assist device validation. *Int. J. Artif. Organs.* 2010;33:446-446

33. Heinke S, Schwandtner S, Siess T, Walter M, Leonhardt S. Development of an innovative mock circulatory loop for vad testing. *Int. J. Artif. Organs.* 2011;34:658-658

34. Pantalos GM, Koenig SC, Gillars KJ, Giridharan GA, Ewert DL. Characterization of an adult mock circulation for testing cardiac support devices. *Asaio J.* 2004;50:37-46

35. Lv X-F, Yang M, Li J-J. Mock circulatory system for performance test of ventricular assist device. *Zhongguo yi liao qi xie za zhi = Chinese journal of medical instrumentation.* 2009;33:313-316

36. Kolyva C, Biglino G, Pepper JR, Khir AW. A mock circulatory system with physiological distribution of terminal resistance and compliance: Application for testing the intra-aortic balloon pump. *Artif. Organs.* 2012;36:E62-E70

37. Legendre D, Fonseca J, Andrade A, Biscegli JF, Manrique R, Guerrino D, Prakasan AK, Ortiz JP, Lucchi JC. Mock circulatory system for the evaluation of left ventricular assist devices, endoluminal prostheses, and vascular diseases. *Artif. Organs.* 2008;32:461-467

38. Vandenberghe S, Shu F, Arnold DK, Antaki JF. A simple, economical, and effective portable paediatric mock circulatory system. *Proc. Inst. Mech. Eng. Part H-J. Eng. Med.* 2011;225:648-656

39. Pantalos GM, Ionan C, Koenig SC, Gillars KJ, Horrell T, Sahetya S, Colyer J, Gray LA. Expanded pediatric cardiovascular simulator for research and training. *Asaio J.* 2010;56:67-72

40. Biglino G, Giardini A, Baker C, Figliola RS, Hsia TY, Taylor AM, Schievano S, Grp MC. In vitro study of the norwood palliation: A patient-specific mock circulatory system. *Asaio J.* 2012;58:25-31

41. Giridharan GA, Koenig SC, Kennington J, Sobieski MA, Chen J, Frankel SH, Rodefeld MD. Performance evaluation of a pediatric viscous impeller pump for fontan cavopulmonary assist. *J. Thorac. Cardiovasc. Surg.* 2013;145:249-257

42. Herreros J, Berjano EJ, Sales-Nebot L, Mas P, Calvo I, Mastrobuoni S, Merce S. A new method of providing pulsatile flow in a centrifugal pump:

Assessment of pulsatility using a mock circulatory system. *Artif. Organs*. 2008;32:490-494

43.   Khalil HA, Kerr DT, Schusterman MA, Cohn WE, Frazier OH, Radovancevic B. Induced pulsation of a continuous-flow total artificial heart in a mock circulatory system. *J. Heart Lung Transplant*. 2010;29:568-573

44.   Farrar DJ, Bourque K, Dague CP, Cotter CJ, Poirier VL. Design features, developmental status, and experimental results with the heartmate iii centrifugal left ventricular assist system with a magnetically levitated rotor. *Asaio J.* 2007;53:310

45.   Cypel M, Yeung JC, Machuca T, Chen MY, Singer LG, Yasufuku K, de Perrot M, Pierre A, Waddell TK, Keshavjee S. Experience with the first 50 ex vivo lung perfusions in clinical transplantation. *J. Thorac. Cardiovasc. Surg.* 2012;144:1200-1207

46.   Nakajima D, Chen FS, Yamada T, Sakamoto J, Ohsumi A, Bando T, Date H. Reconditioning of lungs donated after circulatory death with normothermic ex vivo lung perfusion. *J. Heart Lung Transplant*. 2012;31:187-193

47.   Wigfield CH, Cypel M, Yeung J, Waddell T, Alex C, Johnson C, Keshavjee S, Love RB. Successful emergent lung transplantation after remote ex vivo perfusion optimization and transportation of donor lungs. *Am. J. Transplant*. 2012;12:2838-2844

48.   Mulloy DP, Stone ML, Crosby IK, Lapar DJ, Sharma AK, Webb DV, Lau CL, Laubach VE, Kron IL. Ex vivo rehabilitation of non-heart-beating donor lungs in preclinical porcine model: Delayed perfusion results in superior lung function. *J. Thorac. Cardiovasc. Surg.* 2012;144:1208-1216

49.   Sanchez PG, D'Ovidio F. Ex-vivo lung perfusion. *Curr. Opin. Organ Transpl.* 2012;17:490-495

50.   Wallinder A, Ricksten SE, Hansson C, Riise GC, Silverborn M, Liden H, Olausson M, Dellgren G. Transplantation of initially rejected donor lungs after ex vivo lung perfusion. *J. Thorac. Cardiovasc. Surg.* 2012;144:1222-1228

51.   Hosgood SA, Nicholson ML. First in man renal transplantation after ex vivo normothermic perfusion. *Transplantation*. 2011;92:735-738

52.   Petersen B, Ramackers W, Lucas-Hahn A. Transgenic expression of human heme oxygenase-1 in pigs confers resistance against xenograft rejection during ex vivo perfusion of porcine kidneys (vol 18, pg 355, 2011). *Xenotransplantation*. 2012;19:212-212

53.   Renner P, Eggenhofer E, Popp F, Geissler E, Schlitt HJ, Dahlke MH. Feasibility of continuous ex vivo kidney perfusion with mesenchymal stem cells to prevent ischemia-reperfusion injury in mice. *Transpl. Int.* 2012;25:11-11

54.   Davidson EH, Reformat DD, Allori A, Canizares O, Wagner IJ, Saadeh PB, Warren SM. Flow perfusion maintains ex vivo bone viability: A novel model for bone biology research. *J. Tissue Eng. Regen. Med.* 2012;6:769-776

55. Dragu A, Kleinmann JA, Taeger CD, Birkholz T, Schmidt J, Geppert CI, Prabst K, Unglaub F, Munch F, Weyand M, Kneser U, Horch RE. Immunohistochemical evaluation after ex vivo perfusion of rectus abdominis muscle flaps in a porcine model. *Plast. Reconstr. Surg.* 2012;130:265E-273E

56. Goeden N, Bonnin A. Ex vivo perfusion of mid-to-late-gestation mouse placenta for maternal-fetal interaction studies during pregnancy. *Nat. Protoc.* 2013;8:66-74

57. Hessheimer AJ, Fondevila C, Garcia-Valdecasas JC. Extracorporeal machine liver perfusion: Are we warming up? *Curr. Opin. Organ Transpl.* 2012;17:143-147

58. Izamis ML, Berendsen TA, Uygun K, Yarmush ML. Addressing the donor liver shortage with ex vivo machine perfusion. *J. Healthc. Eng.* 2012;3:279-297

59. Nassar A, D'Amico G, Grady P, Otto M, Dympna K, Zhu X, Fung J, Miller C, Quintini C. Establishing a liver ex-vivo normothermic perfusion model: Lessons learned. *Transpl. Int.* 2012;25:31-31

60. Schreiter T, Marquitan G, Darnell M, Sowa JP, Brocker-Preuss M, Andersson TB, Baba HA, Furch M, Arteel GE, Mathe Z, Treckmann J, Gerken G, Gieseler RK, Canbay A. An ex vivo perfusion system emulating in vivo conditions in noncirrhotic and cirrhotic human liver. *J. Pharmacol. Exp. Ther.* 2012;342:730-741

61. Smith JA, Julius J, Tindall A, Refuerzo J, Berens PD, Moise K. Evaluation of the maternal-fetal transfer of granisetron in an ex vivo placenta perfusion model. *Pharmacotherapy*. 2012;32:E241-E241

62. Ozeki T, Kwon MH, Collins MJ, Brassil JM, Pierson RN, Griffith BP, Poston RS. Heart preservation using continuous ex vivo perfusion improves viability and functional recovery in comparison to cold storage. *J. Heart Lung Transplant.* 2006;25:S115-S116

63. Ozeki T, Kwon MH, Gu JY, Collins MJ, Brassil JM, Miller MB, Gullapalli RP, Zhuo JC, Pierson RN, Griffith BP, Poston RS. Heart preservation using continuous ex vivo perfusion improves viability and functional recovery. *Circ. J.* 2007;71:153-159

64. Colah S, Freed DH, Mundt P, Germscheid S, White P, Ali A, Tian G, Large S, Falter F. Ex vivo perfusion of the swine heart as a method for pre-transplant assessment. *Perfusion-UK*. 2012;27:408-413

65. Collins MJ, Ozeki T, Burris NS, Pierson RN, Griffith BP, Poston RS. Use of continuous ex vivo perfusion to resuscitate hearts after warm ischemia: Animal studies with clinical validation. *J. Heart Lung Transplant.* 2007;26:S64-S65

66. Collins MJ, Ozeki T, Kwon M, Pierson RN, Poston RS. Ex vivo continuous perfusion allows for evaluation of hearts from nonbeating donor hearts. *J. Heart Lung Transplant.* 2006;25:S102-S103

67. Suehiro K, Mohri M, Yamaguchi H, Takagaki M, Hisamochi K, Morimoto T, Sano S. Posttransplant function of a nonbeating heart is predictable by an ex vivo perfusion method. *Ann. Thorac. Surg.* 2001;71:278-283

68. Smulowitz PB, Serna DL, Beckham GE, Milliken JC. Ex vivo cardiac allograft preservation by continuous perfusion techniques. *Asaio J.* 2000;46:389-396

69. Wang DH, Kleist C, Ehser S, Opelz G, Terness P. Ex vivo perfusion with mitomycin c containing solution prolongs heart graft survival in rats. *Transplantation.* 2006;82:1537-1540

70. Scott-Drechsel D, Su ZB, Hunter K, Li M, Shandas R, Tan W. A new flow co-culture system for studying mechanobiology effects of pulse flow waves. *Cytotechnology.* 2012;64:649-666

71. Benbrahim A, Litalien GJ, Milinazzo BB, Warnock DF, Dhara S, Gertler JP, Orkin RW, Abbott WM. A compliant tubular device to study the influences of wall strain and fluid shear-stress on cells of the vascular wall. *J. Vasc. Surg.* 1994;20:184-194

72. Zhao S, Suciu A, Ziegler T, Moore JE, Bürki E, Meister J-J, Brunner HR. Synergistic effects of fluid shear stress and cyclic circumferential stretch on vascular endothelial cell morphology and cytoskeleton. *Arteriosclerosis, Thrombosis, and Vascular Biology.* 1995;15:1781-1786

73. Nakadate H, Hirose Y, Sekizuka E, Minamitani H. A new in vitro pulsatile perfusion system that mimics physiological transmural pressure and shear stress in any size of in vivo vessel. *Journal of Biomechanical Science and Engineering.* 2008;3

74. Peng XQ, Recchia FA, Byrne BJ, Wittstein IS, Ziegelstein RC, Kass DA. In vitro system to study realistic pulsatile flow and stretch signaling in cultured vascular cells. *Am. J. Physiol.-Cell Physiol.* 2000;279:C797-C805

75. Conklin BS, Surowiec SM, Lin PH, Chen C. A simple physiologic pulsatile perfusion system for the study of intact vascular tissue. *Medical engineering & physics.* 2000;22:441-449

76. Gan LM, Sjogren LS, Doroudi R, Jern S. A new computerized biomechanical perfusion model for ex vivo study of fluid mechanical forces in intact conduit vessels. *J. Vasc. Res.* 1999;36:68-78

77. Mironov V, Kasyanov V, McAllister K, Oliver S, Sistino J, Markwald R. Perfusion bioreactor for vascular tissue engineering with capacities for longitudinal stretch. *Journal of Craniofacial Surgery.* 2003;14:340

78. Rey J, Probst H, Mazzolai L, Bosman FTB, Pusztaszeri M, Stergiopulos N, Ris HB, Hayoz D, Saucy F, Corpataux JM. Comparative assessment of intimal hyperplasia development after 14 days in two different experimental settings: Tissue culture versus ex vivo continuous perfusion of human saphenous vein. *J. Surg. Res.* 2004;121:42-49

79. Dummler S, Eichhorn S, Tesche C, Schreiber U, Voss B, Deutsch MA, Hauner H, Lahm H, Lange R, Krane M. Pulsatile ex vivo perfusion of human saphenous vein grafts under controlled pressure conditions increases mmp-2 expression. *Biomed. Eng. Online.* 2011;10

80. Ligush J, Labadie RF, Berceli SA, Ochoa JB, Borovetz HS. Evaluation of endothelium-derived nitric-oxide mediated vasodilation utilizing exvivo perfusion of an intact vessel. *J. Surg. Res.* 1992;52:416-421

81. Saucy F, Probst H, Alonso F, Bérard X, Déglise S, Dunoyer-Geindre S, Mazzolai L, Kruithof E, Haefliger J-A, Corpataux J-M. Ex vivo pulsatile perfusion of human saphenous veins induces intimal hyperplasia and increased levels of the plasminogen activator inhibitor 1. *European Surgical Research*. 2010;45:50-59

82. Maruta F, Parker AL, Fisher KD, Murray PG, Kerr DJ, Seymour LW. Use of a phage display library to identify oligopeptides binding to the lumenal surface of polarized endothelium by ex vivo perfusion of human umbilical veins. *J. Drug Target*. 2003;11:53-59

83. Bergh N, Ekman M, Ulfhammer E, Andersson M, Karlsson L, Jern S. A new biomechanical perfusion system for ex vivo study of small biological intact vessels. *Ann. Biomed. Eng.* 2005;33:1808-1818

84. Ising M, Warren S, Sobieski M, Slaughter M, Koenig S, Giridharan G. Flow modulation algorithms for continuous flow left ventricular assist devices to increase vascular pulsatility: A computer simulation study. *Cardiovascular Engineering and Technology*. 2011:1-11

85. Ising M, Warren S, Sobieski M, Slaughter M, Koenig S, Giridharan G. Flow modulation algorithms for continuous flow left ventricular assist devices to increase vascular pulsatility: A computer simulation study. *Cardiovascular Engineering and Technology*. 2011;2:90-100

86. Schroeder MJ, Perreault B, Ewert DL, Koenig SC. Heart: An automated beat-to-beat cardiovascular analysis package using matlab((r)). *Comput. Biol. Med.* 2004;34:371-388

87. Slaughter MS, Pagani FD, Rogers JG, Miller LW, Sun B, Russell SD, Starling RC, Chen LW, Boyle AJ, Chillcott S, Adamson RM, Blood MS, Camacho MT, Idrissi KA, Petty M, Sobieski M, Wright S, Myers TJ, Farrar DJ, HeartMate IIC. Clinical management of continuous-flow left ventricular assist devices in advanced heart failure. *J. Heart Lung Transplant.* 2010;29:S1-S39

88. Ford MD, Alperin N, Lee SH, Holdsworth DW, Steinman DA. Characterization of volumetric flow rate waveforms in the normal internal carotid and vertebral arteries. *Physiological Measurement*. 2005;26:477-488

89. Gwilliam MN, Hoggard N, Capener D, Singh P, Marzo A, Verma PK, Wilkinson ID. Mr derived volumetric flow rate waveforms at locations within the common carotid, internal carotid, and basilar arteries. *J. Cereb. Blood Flow Metab.* 2009;29:1975-1982

90. Busse R, Fleming I. Pulsatile stretch and shear stress: Physical stimuli determining the production of endothelium-derived relaxing factors. *J Vasc Res.* 1998;35:73-84

91. Estrada R, Giridharan GA, Nguyen MD, Roussel TJ, Shakeri M, Parichehreh V, Prabhu SD, Sethu P. Endothelial cell culture model for replication of physiological profiles of pressure, flow, stretch, and shear stress in vitro. *Anal. Chem.* 2011;83:3170-3177

92. Fisher AB, Chien S, Barakat AI, Nerem RM. Endothelial cellular response to altered shear stress. *Am. J. Physiol.-Lung Cell. Mol. Physiol.* 2001;281:L529-L533

93. Inoue N, Ramasamy S, Fukai T, Nerem RM, Harrison DG. Shear stress modulates expression of cu/zn superoxide dismutase in human aortic endothelial gels. *Circ.Res.* 1996;79:32-37

94. Li Y, Zheng J, Bird IM, Magness RR. Mechanisms of shear stress-induced endothelial nitric-oxide synthase phosphorylation and expression in ovine fetoplacental artery endothelial cells. *Biol. Reprod.* 2004;70:785-796

95. Li YSJ, Haga JH, Chien S. Molecular basis of the effects of shear stress on vascular endothelial cells. *J. Biomech.* 2005;38:1949-1971

96. Martinez A, Arias J, Bassuk JA, Wu H, Kurlansky P, Adams JA. Adrenomedullin is increased by pulsatile shear stress on the vascular endothelium via periodic acceleration (pgz). *Peptides.* 2008;29:73-78

97. Nakata M, Tatsumi E, Tsukiya T, Taenaka Y, Nishimura T, Nishinaka T, Takano H, Masuzawa T, Ohba K. Augmentative effect of pulsatility on the wall shear stress in tube flow. *Artif. Organs.* 1999;23:727-731

98. Soucy KG, Ryoo S, Benjo A, Lim HK, Gupta G, Sohi JS, Elser J, Aon MA, Nyhan D, Shoukas AA. Impaired shear stress-induced nitric oxide production through decreased nos phosphorylation contributes to age-related vascular stiffness. *J. Appl. Physiol.* 2006;101:1751

99. Thacher T, Gambillara V, Da Silva R, Montorzi G, Stergiopulos N, Silacci P. Oscillatory shear stress and reduced compliance impair vascular functions. *Clinical hemorheology and microcirculation.* 2007;37:121-130

100. Tinken TM, Thijssen DHJ, Hopkins N, Black MA, Dawson EA, Minson CT, Newcomer SC, Laughlin MH, Cable NT, Green DJ. Impact of shear rate modulation on vascular function in humans. *Hypertension.* 2009;54:278-285

101. Traub O, Berk BC. Laminar shear stress - mechanisms by which endothelial cells transduce an atheroprotective force. *Arterioscler. Thromb. Vasc. Biol.* 1998;18:677-685

102. Drugs.com. Normosol-r injection. 2009;2013

103. Cutnell J, Johnson K. *Physics.* Wiley.

104. Kesmarky G, Kenyeres P, Rabai M, Toth K. Plasma viscosity: A forgotten variable. *Clinical Hemorheology and Microcirculation.* 2008;39:243-246

105. Lab MV. Whole blood viscosity vs. Serum and plasma viscosity. 2013;2013

106. Sabbah HN, Anbe DT, Stein PD. Negative intraventricular diastolic pressure in patients with mitral-stenosis - evidence of left-ventricular diastolic suction. *Am. J. Cardiol.* 1980;45:562-566

Mitchell J. Buller
Graduate Student
Department of Bioengineering
University of Louisville
Research Assistant
Cardiovascular Innovation Institute
Louisville, Kentucky, USA
859-760-7050
mjbull01@louisville.edu

Education

Future (Fall 2013)   University of Louisville
School of Medicine
Class of 2017

2012 – Present   University of Louisville
J.B. Speed School of Engineering
Master of Engineering
Department of Bioengineering
With High Honors

2008 – 2012   University of Louisville
J.B. Speed School of Engineering
Bachelor of Science
Department of Bioengineering
With High Honors

Research Experience

2012 – Present   Cardiovascular Innovation Institute
Mentors: Mark Slaughter, MD; Steven Koenig,
PhD; Guruprasad Giridharan, PhD; Kevin
Soucy, PhD; Michael Sobieski, RN, CCP

- Investigated effects of novel mechanical circulatory support devices in bovine and mock flow loop models
- Trained in clinical and animal blood and tissue harvesting and histological and pathological assessment
- Trained in instrumentation, data acquisition and analysis, and developing experimental protocols for acute and chronic device testing
- Trained in-vitro hemolysis testing for FDA IDE and 510K approvals

Work Experience

2010 – 2011	Ethicon Endo-Surgery Cincinnati, OH Co-op Directors: Kevin Doll, Tony Nguyen, Catherine Corbett

- Data analysis using Minitab and Excel software
- Mechanical testing for compressive, tensile, and torsional loads
- Tolerance stack-ups
- Predictive and applied failure analysis
- Professional written communication via engineering studies

Peer Reviewed Conference Presentations

Slaughter, MS; Sobieski, MA; **Buller, MJ**; McCants, K; Burkes, E. *Single Center Experience with Formation of Ring Thrombus on Inlet Bearing with Axial Flow Left Ventricular Assist Device*. 58th Annual ASAIO Conference, San Francisco, CA, 2012.

Buller, MJ; Sobieski, MA; Soucy, KG; Giridharan, GA; Koenig, SC; Slaughter, MS. *Investigation of myocardial recovery in a chronic ischemic heart failure bovine model*. 39th Annual ESAO Conference, Rostock, Germany, 2012.

Soucy, KG; Ansert, AC; Holley, KP; Spalding, CT; Benzinger, CJ; **Buller, MJ**; Giridharan, GA; Koenig, SC; Sobieski, MA; Slaughter, MS. *Feasibility of Ventricular-Arterial Cannula for Aortic Valve Bypass*. 2012 BMES Annual Meeting, Atlanta, GA.

Honors and Awards

1. Dean's List and Dean's Scholar
2. Pi Kappa Alpha Member of the Year, 2012
3. Tau Beta Pi Engineering Honor Society

Campus Involvement and Community Service

1. Pi Kappa Alpha fraternity
2. U of L Dance Marathon
3. U of L Relay for Life
4. Alternative Spring Break
5. Ken-ducky Derby
6. Prevent Child Abuse America
7. Make A Wish Foundation
8. Big Brothers Big Sisters of Kentuckiana
9. WHAS Crusade for Children